PHYSICAL REVIEW D VOLUME 35, NUMBER 1 1 JANUARY 1987

Analysis of the decay mechanism of dibaryon resonances

N. Konno and H. Nakamura
Department of Physics, College of Science and Engineering, Aoyama Gakuin University, Setagaya, Tokyo 157, Japan

H. Noya
Institute of Physics, Faculty of Economics, Hosei University at Tama, Machida, Tokyo 194-02, Japan
(Received 19 May 1986; revised manuscript received 17 June 1986)

Using phenomenological methods, we analyze the decay mechanism for dibaryon resonances based on the diquark-cluster model, and discuss the possibility of observing the following states: $I=0$ and $J^P=1^+$ at 2.08 and 2.14 GeV c.m. energy; $I=0$ and $J^P=3^-$ at 2.25 GeV; and $I=1$ and $J^P=0^+$ at 2.02, 2.08, and 2.14 GeV. The analysis leads us to the conclusion that the decay of dibaryons can be attributed to the production of a pion followed by the transformation of the system. We describe the dynamics of the decay by the use of an effective interaction V_π which involves the operators of one-pion production and a system transformation. All the parameters in V_π are determined by the use of the experimental data concerning $I=1$ dibaryons. When an appropriate fine structure for the mass spectrum in the diquark-cluster model is chosen, the P_1 πd phase shift (T matrix) calculated using V_π is in close agreement with reported phase-shift-analysis data [$B_1^2(2.14)1^+$]. The predictions of the present model are quite consistent with the existing data both for the narrow dibaryon resonances observed in various reactions, as well as for the broad dibaryon resonances.

I. INTRODUCTION

One of the most interesting problems in intermediate-energy physics is the existence of NN and/or πd resonances, the dibaryon.[1-3] This is a problem both for the theorist and for the experimenter. Briefly, the problem lies in explaining the structure of a dibaryon. There are two compelling approaches to understanding the dibaryon. In one approach, the dibaryon is interpreted as a πNN three-body resonating state[4,5] on the basis of a Faddeev calculation, and in the other, the dibaryon is viewed as a six-quark bound state q^6 (Refs. 6—11). Since 1977 the latter view has been emphasized by Yokosawa in his path-breaking experimental works.[2,3] Many πd scattering experiments have been carried out in the energy regions where two established dibaryons $B_1^2(2.14)2^+$ (Refs. 1—3 and 12—14) and $B_1^2(2.22)3^-$ (Refs. 1—3 and 13—15) exist, in order to measure both the vector analyzing power iT_{11} (Refs. 16 and 17) and the tensor polarization T_{20} (Refs. 18—21). In the measurements of iT_{11} (Ref. 17) the experimental values have agreed fairly well with the predictions of the πNN model and supporting evidence for the q^6 model has not been obtained. One result, suggested by Yokosawa[22] and Hoshizaki,[23] that would be favorable for the q^6 model, would be the existence of a $B_0^2(2.22)3^-$ having a rather narrow decay width: $\Gamma\sim 50$ MeV (Ref. 23). But this dibaryon resonance has not yet been established experimentally. Based on these facts, some authors have suggested the possibility that all dibaryon resonances can be explained solely by using the πNN model.

However this situation was changed by the work of the ETH group,[20,21] who reported the discovery of a new dibaryon resonance of $B_1^2(2.14)1^+$ with a very narrow width of 10—30 MeV, together with a broad dibaryon resonance of a $B_1^2(2.14)2^+$. Since the existence of the dibaryon with such a narrow decay width has never been predicted by the πNN model, it has been suggested that the q^6 model advanced by Yokosawa should be revived as an alterative. Although the presence of this dibaryon has not been completely confirmed yet, one can say at least that the q^6 model has recovered some of its experimental base. This viewpoint has been supported by reports on missing-mass[24] and invariant-mass experiments[25] using light nuclei in which several narrow dibaryon resonances have been observed. Yokosawa's experimental analysis with respect to the $B_0^2(2.22)3^-$ dibaryon may also support this viewpoint. Considering that a new experimental analysis of np scattering[26] has started in LAMPF for the purpose of establishing of the $B_0^2(2.22)3^-$ dibaryon and finding other $I=0$ dibaryons with narrow widths, it is very appropriate to present a theoretical analysis and predictions for the properties of dibaryon resonances based on a q^6 model. The present analysis is one such attempt and is based on the diquark-cluster model[11] that we proposed previously.

There are two major tasks for any model of dibaryon resonances, the reproduction of experimental data concerning both the mass spectrum and partial decay widths. As will be discussed in Sec. II, our prediction using the diquark-cluster model for the mass spectrum agrees well with the experimental analysis of Yokosawa.[2,3] At present our analysis concerning the mass spectrum is consistent with all reported experimental data.[2,3] It should be noted that at present the diquark-cluster model is the only

theory which can explain why the $B_1^2(2.14)1^+$ and $B_1^2(2.14)2^+$ have the same masses as the $B_0^2(2.22)3^-$ and $B_1^2(2.22)3^-$. Concerning the second problem, explaining the experimental data on partial decay widths, there are no reliable methods for calculating the partial decay widths $\Gamma^{\pi NN}$, $\Gamma^{\pi d}$, and Γ^{NN} for the πNN, πd, and NN channels based on the q^6 model. In fact, even the diquark-cluster model based on QCD gives us little information on the details of the dynamics which dominate the decay process of the q^6 system. For this reason, we make a phenomenological analysis for the dynamic part of the decay mechanism. The kinematic part related to the structure of the q^6 system is analyzed exactly using the diquark-cluster model. Of course, in such an analysis, those observable phenomena which are less dependent on the uncertain dynamic aspect are likely to be more consistent with the experiment data.

In this paper we first analyze the reported Γ and Γ^{NN} data for the $B_1^2(2.14)2^+$ and $B_1^2(2.22)3^-$ and also the $\Gamma^{\pi NN}$ and Γ^{NN} data for $B_0^2(2.22)3^-$. Then, we set up a scheme for the decay dynamics which may be able to reproduce these experimental data. We describe the decay dynamics by the use of an effective interaction V_π and calculate the partial decay widths $\Gamma^{\pi NN}$, $\Gamma^{\pi d}$, and Γ^{NN} with the use of V_π. The parameters in V_π are determined by the use of the experimental data for $I=1$ dibaryons. The P_1 πd phase shift (T matrix) calculated using V_π depends strongly on the fine structure of the energy level of $B_1^2(2.14)1^+$, in which four states are degenerate in the diquark cluster model. We present a promising case in which the theoretical T matrix agrees well with the experimental one. Finally we predict the NN and πd T matrices for some low-lying dibaryons, which are indicated by the diquark cluster model but have not yet been observed by phase-shift analysis. In this work we attempt to provide some guidance for those conducting experiments.

This paper consists of seven sections. In Sec. II we review the diquark-cluster model. In Sec. III we discuss the decay mechanism of the dibaryon and introduce the V_π. In Sec. IV we establish the calculation method for the partial decay widths of $\Gamma^{\pi NN}$, $\Gamma^{\pi d}$, and Γ^{NN}. The method to calculate the NN and πd phase shifts (T matrices) under the influence of a group of dibaryons is given in Sec. V. A comparison of our predictions with experimental observations is provided in Sec. VI. Some comments on further analysis are given in Sec. VII.

II. DIQUARK-CLUSTER MODEL

As discussed in Sec. I we will calculate the partial decay widths of the dibaryon by using the diquark-cluster model[11] for the structure of the q^6 system. In this section we summarize the ideas of the diquark-cluster model and add some speculations on the high excitation state of the q^6 system.

The diquark cluster model is fundamentally based on the shell model with a jj-coupling scheme like the nuclear shell model and also based on a cluster model of quarks which Lichtenberg *et al.*[27] developed from the string model. The color configuration of six quarks in the diquark-cluster model is illustrated in Fig. 1. As in the nuclear shell model, the dibaryon mass spectrum is given by the following simple equation:

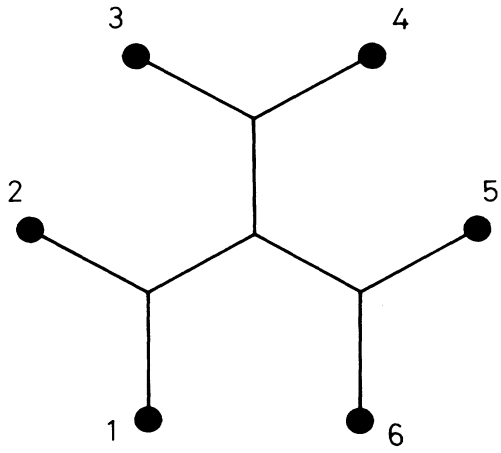

FIG. 1. The color configuration of six quarks in the diquark-cluster model. This system consists of three diquarks (12), (34), and (56). Two quarks in a diquark are tightly bound and make a diquark cluster only in the case where both of them are in $1s\frac{1}{2}$ shell.

$$M = 6m + M(p\tfrac{1}{2})n(p\tfrac{1}{2}) + M(p\tfrac{3}{2})n(p\tfrac{3}{2}) + M(d\tfrac{3}{2})n(d\tfrac{3}{2}) + \delta_3^{12}(qq) + \delta_3^{34}(qq) + \delta_3^{56}(qq)\ . \tag{2.1}$$

Here $M(lj)$ is the single-particle excitation energy from the $1s\frac{1}{2}$ shell to the shell with the orbital angular momentum l and total angular momentum j, and $n(lj)$ indicates the number of quarks in the shell. The excitation for the shell characterized by $j > \frac{3}{2}$ is neglected. In accordance with the nuclear shell model, a harmonic-oscillator potential is taken as the common central force, in addition to a common induced LS force. The excitation energy $M(lj)$ is a function of the quark mass m and the angular frequency ω. It is assumed that the interaction energy $\delta_3^{ij}(qq)$ in the (diquark) system of two quarks, i and j, whose color state is the $\mathbf{3}^*$ state, takes a nonvanishing value when they are in the $1s\frac{1}{2}$ shell. In other words, two quarks in a diquark are tightly bound to make a cluster (diquark cluster) only if both of them are in the $1s\frac{1}{2}$ shell. The interaction energy $\delta_3^{ij}(qq)$ for the diquark cluster depends on the spin of the system and its value is determined by using the mass of N and Δ. The values for parameters m and ω adopted by the authors[28–30] are both around 0.3 GeV. Setting $m=\omega$, we adjusted the parameter m to reproduce the resonating energy 2.14 GeV of $B_1^2(2.14)2^+$ and obtained $m=0.300$ GeV. Using these parameters, the calculated mass spectrum are shown in Fig. 2 together with a list of experimental dibaryon candidates.

The dibaryon in which the quarks are excited only to the $1p\frac{1}{2}$ shell is referred to as the $1p\frac{1}{2}$-shell dibaryon. In Fig. 2, all of low-lying $1p\frac{1}{2}$-shell dibaryons with rest mass below ~ 2.3 GeV are given. As for the high-lying levels above ~ 2.3 GeV, we illustrate a series of dibaryons

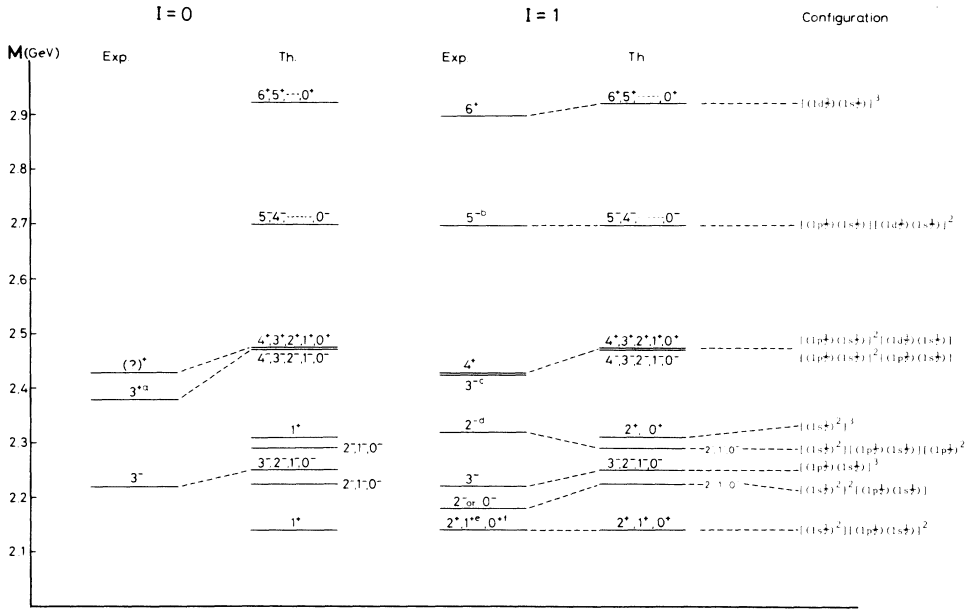

FIG. 2. The mass spectrum of dibaryons and the predictions of the diquark-cluster model with the respective configurations. The predicted spectrum is independent of the isospin I of system. The experimental data are from Ref. 3 but (a) from Ref. 33, (b) NN spin-triplet $J=L=$odd state, assumed to be $J=5$, (c) NN spin-triplet $J=L=$odd state, assumed to be $J=3$, (d) from Ref. 40, (e) from Ref. 20, (f) from Ref. 39, NN spin-singlet $J=L=$even state, assumed to be $J=0$.

($1d\frac{3}{2}$-shell dibaryon) which are obtained by a successive transfer of the quarks in $B^2_{0,1}(2.22)3^-$ from the $1p\frac{1}{2}$ shell to the $1d\frac{3}{2}$ shell. It is very interesting to note that the $1d\frac{3}{2}$-shell dibaryons with maximum angular momentum in the allowed configuration are found in the same position as the dibaryon candidates suggested by Yokosawa.[3] In the diquark-cluster model, the series of $1d\frac{3}{2}$-shell dibaryons should coexist with another series of dibaryons ($1p\frac{3}{2}$-shell dibaryon) having the same mass spectrum, which corresponds to the transfer of quarks from the $1p\frac{1}{2}$ shell to the $1p\frac{3}{2}$ shell. A dibaryon candidate $B^2_1(2.43)(?)^-$ (Ref. 31) found by Yokosawa[2,3,32] can be assigned to a $1p\frac{3}{2}$-shell dibaryon. However, the other member of the $1p\frac{3}{2}$-shell dibaryon has not yet been observed. In a previous paper,[11] we assigned a candidate $B^2_0(2.38)3^+$ (Ref. 33) to a dibaryon with the configuration $[(1p\frac{1}{2})(1s\frac{1}{2})]^2[(1p\frac{1}{2})^2]$. Although the empirical rest mass 2.38 GeV is well reproduced by this assignment, it is also possible to assume that this candidate belongs to a family of $1d\frac{3}{2}$-shell dibaryons, as illustrated in Fig. 2. In fact, the observed energy shift between $B^2_0(2.38)3^+$ and $B^2_0(2.43)(?)^+$ (Refs. 2, 3, and 32) can be understood in terms of the fine structure of the dibaryon mass spectrum, as will be discussed in Sec. VI.

It is inferred from these results that the excitation process of quarks in the q^6 system is dominated by the following rules: (1) At most, three quarks can be excited; (2) the major high-lying states above 2.3 GeV are a series of $1d\frac{3}{2}$-shell dibaryons with the maximum angular momentum in the allowed configuration; (3) the coexisting $1p\frac{3}{2}$-shell dibaryons are less important except in some specific cases. The physical implications of these rules are uncertain at present.

The configurations of the major members in the dibaryons, given in Fig. 2, are listed in Table I. It should be noted that a few $1p\frac{1}{2}$-shell dibaryons exist above 2.3 GeV including the state with the configuration $[(1s\frac{1}{2})^2]^3$ at 2.31 GeV. The reason why these pure S-wave dibaryons lie in a rather-high-energy region (>2.3 GeV) is as follows. The interaction energy $\delta^{ij}_3(qq)$ for the diquark cluster is given by

$$\delta^{ij}_3(qq)=a+b\mathbf{s}_i\cdot\mathbf{s}_j\ , \tag{2.2}$$

where $\mathbf{s}_i$ and $\mathbf{s}_j$ are the spin of the quarks i and j, respectively. The values for the parameters a and b are $a=0.186$ GeV and $b=0.195$ GeV. The state of a diquark is denoted by $[TS]$ where T and S represent the isospin and spin states, respectively. There are two possible states [00] and [11] for the diquark cluster as the constituent quarks are both in $1s\frac{1}{2}$ state. The states [00] and [11] have interaction energies of 0.040 and 0.235 GeV, respectively. Then, by the inclusion of a [11] diquark cluster, the q^6 system acquires a large extra energy 0.235 GeV. The pure S-wave dibaryons must involve at least two [11] diquark clusters because the wave function of the q^6 system is symmetrical for the constituent three diquarks. The resultant large amount of extra energy raises the dibaryon energy level above 2.3 GeV. In another example, the state with the configuration $[(1s\frac{1}{2})^2]^2[(1p\frac{1}{2})(1s\frac{1}{2})]$ acquires an extra energy of 0.235 GeV or more because it involves at least one [11] diquark cluster. This extra energy raises the energy level above 2.2 GeV.

TABLE I. Classification of q^6 states by configuration, isospin I, and spin and parity J^P. Generally a bracket [ ] represents a diquark. For example, notation [TS] indicates the isospin T and spin S states of a diquark. The member of each group is characterized by the [TS] combination of three diquarks with notation A, B, C, and D which indicate the number of $T=1$ diquarks in the system. The contribution of each term of Eq. (2.1) to dibaryon mass E_r ($=M$) is given in GeV explicitly, in the following manner:

(1) (2) (3) (4) (5) (6) (7)

$$E_r = 6m + M(p\tfrac{1}{2})n(p\tfrac{1}{2}) + M(p\tfrac{3}{2})n(p\tfrac{3}{2}) + M(d\tfrac{3}{2})n(d\tfrac{3}{2}) + \delta_3^{12}(qq) + \delta_3^{34}(qq) + \delta_3^{56}(qq) .$$

For $1d\frac{3}{2}$-shell dibaryons, the states with the maximum J in each configuration are shown and, as for the other states, only the state number N is given. Note that $1p\frac{3}{2}$-shell and $1d\frac{3}{2}$-shell dibaryons have the same mass spectrum with the same [TS] combinations, since $M(p\frac{1}{2})=\frac{1}{2}m$ and $M(p\frac{3}{2})=M(d\frac{3}{2})=\frac{5}{4}m$.

I	J^P	Configuration [TS] combination									
		$1p\frac{1}{2}$-shell dibaryons									
		$[(1s\frac{1}{2})^2]^3$	$E_r=1.800+0+0+0+0.040+0.235+0.235=2.310$								
1	2^+	C [00][11][11]									
	0^+	C [00][11][11]									
0	1^+	C [00][11][11]									
		$[(1s\frac{1}{2})^2][(1p\frac{1}{2})(1s\frac{1}{2})]$	$E_r=1.800+0.150+0+0+0.040+0.235+0=2.225$								
1	2^-	B [00][11][01]	C	[00][11][11]							
	1^-	B_1 [00][11][01]	B_2	[00][11][00]	C_1	[00][11][11]	C_2	[00][11][10]			
	0^-	B [00][11][01]	C	[00][11][11]							
0	2^-	C [00][11][11]									
	1^-	C_1 [00][11][11]	C_2	[00][11][10]							
	0^-	C [00][11][11]									
		$[(1s\frac{1}{2})^2][(1p\frac{1}{2})(1s\frac{1}{2})]^2$	$E_r=1.800+0.150\times2+0+0+0.040+0+0=2.140$								
1	2^+	B [00][01][11]	C	[00][11][11]							
	1^+	B_1 [00][01][11]	B_2	[00][00][11]	B_3	[00][01][10]	C	[00][11][10]			
	0^+	B_1 [00][01][11]	B_2	[00][00][10]	C_1	[00][11][11]	C_2	[00][10][10]			
0	1^+	A_1 [00][01][01]	A_2	[00][00][01]	C_1	[00][11][11]	C_2	[00][11][10]			
		$[(1p\frac{1}{2})(1s\frac{1}{2})]^3$	$E_r=1.800+0.150\times3+0+0+0+0+0=2.250$								
1	3^-	C [01][11][11]									
	2^-	B_1 [01][01][11]	B_2	[01][00][11]							
		C_1 [01][11][11]	C_2	[00][11][11]	C_3	[01][11][10]					
		D_1 [11][11][11]	D_2	[10][11][11]							
	1^-	B_1 [01][01][11]	B_2	[01][00][11]	B_3	[01][01][10]	B_4	[01][00][10]			
		C_1 [01]{[11][11]}$_{12}$	C_2	[01]{[11][11]}$_{10}$	C_3	[01][11][10]	C_4	[00][11][10]			
		C_5 [01][10][10]									
		D_1 [11][11][11]	D_2	{[11][11]}$_{01}$[10]	D_3	{[11][11]}$_{21}$[10]	D_4	[11][10][10]			
	0^-	B_1 [01][01][11]	B_2	[01][00][11]							
		C_1 [01][11][10]	C_2	[00][11][11]	C_3	[00][10][10]					
		D_1 [11][11][11]	D_2	[11][11][10]							
0	3^-	D [11][11][11]									
	2^-	C_1 [01][11][11]	C_2	[01][11][10]	D	[11][11][10]					
	1^-	A [01][01][00]	C_1	[01][11][11]	C_2	[00][11][11]	C_3	[01][10][11]	C_4	[00][11][10]	
		D_1 [11][11][11]	D_2	[11][10][10]							
	0^-	A [01][01][01]	C	[01][11][11]	D_1	[11][11][10]	D_2	[10][10][10]			
		$[(1s\frac{1}{2})^2][(1p\frac{1}{2})(1s\frac{1}{2})][(1p\frac{1}{2})^2]$	$E_r=1.800+0.150\times3+0+0+0.040+0+0=2.290$								
1	2^-	B [00][01][11]	C	[00][11][11]							
	1^-	B_1 [00][01][11]	B_2	[00][00][11]	B_3	[00][11][00]	C_1	[00][11][11]	C_2	[00][10][11]	
	0^-	B_1 [00][01][11]	B_2	[00][10][00]	C	[00][11][11]					
0	2^-	C [00][11][11]									
	1^-	A [00][01][00]	C_1	[00][11][11]	C_2	[00][10][11]					
	0^-	A [00][00][00]	C	[00][11][11]							

TABLE I. (*Continued*).

$1d\frac{3}{2}$-shell dibaryons with the maximum J

Configuration	$E_r=(1)+(2)+(3)+(4)+(5)+(6)+(7)$
$[(1p\frac{1}{2})(1s\frac{1}{2})]^2[(1d\frac{3}{2})(1s\frac{1}{2})]$	$E_r=1.800+0.150\times2+0+0.375+0+0+0=2.475$
$I=1$, $J^P=4^+$	
B [01][11][02]	C_1 [01][11][12] C_2 [11][11][02] D [11][11][12]
$I=0$, $J^P=4^+$	
C [01][11][12]	D [11][11][12]
$[(1p\frac{1}{2})(1s\frac{1}{2})][(1d\frac{3}{2})(1s\frac{1}{2})]^2$	$E_r=1.800+0.150+0+0.375\times2+0+0+0=2.700$
$I=1$, $J^P=5^-$	
B [01][02][12]	C_1 [01][12][12] C_2 [11][02][12] D [11][12][12]
$I=0$, $J^P=5^-$	
C [11][02][12]	D [11][12][12]
$[(1d\frac{3}{2})(1s\frac{1}{2})]^3$	$E_r=1.800+0+0+0.375\times3+0+0+0=2.925$
$I=1$, $J^P=6^+$	
C [02][12][12]	
$I=0$, $J^P=6^+$	
D [12][12][12]	

State number N of $1d\frac{3}{2}$-shell dibaryons with the configuration $[(1p\frac{1}{2})(1s\frac{1}{2})]^{3-\alpha}[(1d\frac{3}{2})(1s\frac{1}{2})]^{\alpha}$

	$I=1$				$I=0$		
$J\backslash\alpha$	1	2	3	$J\backslash\alpha$	1	2	3
0	18	27	12	0	10	15	8
1	44	62	31	1	24	35	17
2	44	67	37	2	24	37	19
3	22	49	29	3	12	27	17
4	4	22	17	4	2	12	9
5		4	7	5		2	3
6			1	6			1

Here we make a short comment on the physical implications of the parameter a, which experimentally takes a positive value 0.186 GeV and vanishes as the diquark is excited. In Lichtenberg's model,[27] the excited q^6 system has a rodlike shape and the parameter a represents the color-flux energy of the diquark cluster at the ends of the system. Consequently, the sign of parameter a should be positive but the magnitude may increase as the diquark cluster is excited. In the usual shell-model picture, however, the cluster is enveloped by the system and is formed by the attractive short-range residual interaction between particles. Adopting this picture for the diquark cluster model, the parameter a represents the binding energy of a diquark cluster in the q^6 system and therefore the sign would be negative though the magnitude would be reduced as the diquark cluster is excited. It is an open question concerning the shell-model picture as to why the parameter a is positive.

III. DYNAMICS OF THE DECAY PROCESS OF DIBARYONS

In this section we provide a phenomenological analysis of dibaryon resonances based on the diquark-cluster model, and develop the discussion with the use of experimental data for the two dibaryons $B_1^2(2.14)2^+$ and $B_1^2(2.22)3^-$. In the context of the discussion we assume the existence of the $B_0^2(2.22)3^-$ and adopt the results of Hoshizaki's analysis.[23] Although this dibaryon has not been experimentally established yet, it is natural for us to use the data because it is one of major members of the dibaryons that are predicted by the diquark-cluster model. From the phenomenological point of view, we point out that as a q^6 picture is adopted for dibaryon resonances there are generally two critical problems concerning the mechanism of dibaryon decay.

(1) Since a q^6 system is of small size generally, the emission of a low-energy particle with high orbital angular momentum is suppressed strongly. This indicates that the decay widths Γ for the dibaryons with high angular momenta and low-Q values are rather small. For two major dibaryons $B_1^2(2.14)2^+$ and $B_1^2(2.22)3^-$, the experimental values for Γ are ~70 and ~140 MeV, respectively. These values seem to be inconsistent with the above simple conjecture. In order to fit the theory to the experiment, the effective radius of the dibaryon should be much larger than anticipated from mass spectrum data.

(2) The experimental value for $\Gamma^{\pi NN}$ of the $B_0^2(2.22)3^-$ is not so small compared with that of the $B_1^2(2.22)3^-$. In fact, the $\Gamma^{\pi NN}\sim40$ MeV obtained by Hoshizaki's phase-shift analysis[23] amounts to almost $\frac{1}{3}$ of that of the $B_1^2(2.22)3^-$. It is usually thought that the decay of the q^6

to the πNN channel occurs mainly via a one-pion-production process from the Δ in $N\Delta$ intermediate state, with a strong enhancement due to Δ resonance. However, the large width of $B_0^2(2.22)3^-$ is difficult to justify by this approach since the $N\Delta$ intermediate state is not allowed for $I=0$ cases.

There may, of course, be separate factors causing each of these two difficulties. In this paper, however, we try to solve those two problems simultaneously. We are motivated by a bag-model picture presented by Ui and Saito[34] recently. They suggested that the deformation of a bag can take place easily and that the original form of the bag is preserved by the high pressure of the virtual-pion field outside the bag which has been discussed by many authors.[35–37] We apply this idea to the q^6 system described by the diquark-cluster model.

Our modeling of the decay process of the q^6 system follows. Imagine a q^6 system, at first, without a virtual-pion field outside. The q^6 system immediately starts to transform and may become a rodlike shape due to centrifugal force. It is natural to consider that the quarks which have moved independently are collected into two clusters at both ends of this transformed q^6 system. If both of the end clusters are baryons, the major part of the color-electric force vanishes and it cannot bring the system back to the original state, and the fission of the system occurs. In the real q^6 system, however, the pressure of the virtual-pion field outside operates in this step as a restorative force and thus the fission of the system is prevented. But what will happen if a real pion is emitted from the baryon cluster immediately before the restorative force operates? It may be that the virtual-pion field is considerably disturbed and any restorative action is inhibited. The transformation of the system would then proceed. When the emitted real pion leaves, the virtual-pion field becomes stable, but the q^6 system does not return to its original state and ultimately fissions into two baryons. Pion emission is thus characteristic of the decay mechanism. The mechanism can be summarized as follows.

(A) The decay of the dibaryon is initiated by the emission of a pion from a baryon cluster that is in either of the two ends of a rod-shaped transformed q^6 system. The q^6 system then continues to transform until it results in a fission. There is no direct transition to the channels where a pion is not involved (NN, $N\Delta$, $\Delta\Delta$ channels).

In this picture it is almost self-evident that the above-mentioned two problems automatically resolve themselves. The q^6 system transforms immediately before decaying and the distance between the baryon clusters becomes large and a pion is not produced by way of Δ but directly produced from the q^6.

Assuming the mechanism (A) for the decay of the q^6, the transition to the NN channel comes as a secondary effect. It must occur via the reabsorption of the pion emitted from q^6 by one of the produced baryons. Generally, the matrix element for the transition to a channel becomes a strongly decreasing function of the momenta of the emitted particles when the system expands as in process (A). Since the momentum in the NN channel is considerably larger than the momenta of the particles in the other channels, the matrix element for the NN channel should be smaller than the others. This would explain the relative smallness of Γ^{NN}.

Here we briefly explain the phenomenological implications of the mechanism by which the matrix element for the NN channel decreases. We take out of the configuration which consists of two baryon clusters B_c and B_c' in the q^6 system, the relative orbital angular momentum between B_c and B_c' is represented by l. The q^6 models can be classified into two groups with respect to L, the maximum value of l. One group involves the $B_1^2(2.14)2^+$ and $B_1^2(2.22)3^-$ corresponding to $L=0$ and $L=1$, respectively. The other involves the same states but with $L=2$ and $L=3$, respectively. Our diquark-cluster model belongs to this second group.

The experimental result for the ratio $\Gamma^{NN}/\Gamma^{\pi NN}$ is quite small (about 0.2). Since the orbital angular momentum in the NN channel is $L+2$ in the first group of models, transition to the NN channel accompanies a change in orbital angular momentum. This may be consistent with the above experimental finding because in such cases the transition is generally suppressed. In contrast, in the second group the transition to the NN channel can occur without the change in orbital angular momentum and therefore the transition may be superallowed. This contradicts the experimental finding. This small ratio $\Gamma^{NN}/\Gamma^{\pi NN}$ can only be explained by rather restrictive assumptions concerning the decay mechanism. The decay mechanism (A) proposed in this paper incorporates these assumptions.

The next question involves the determination of the effective interaction V_π from the process (A), which describes the dynamic part of the decay process of the dibaryon. Hereafter the term Ψ^B will be used to denote one component of the q^6 wave function Ψ, a two-baryon cluster without internal excitation. The B_c and B_c' in Fig. 3 represent the baryon cluster that emits a pion and the spectator cluster, respectively. The momenta of the pion and the B_c' in the c.m. system are $\mathbf{q}$ and $-\mathbf{h}$, and the momenta of B_c, before and after the production of the pion, are $\mathbf{h}$ and $\mathbf{h}'$ $(=\mathbf{h}-\mathbf{q})$, respectively. Using the momentum representation, the component Ψ^B is written as $\Psi^B(\mathbf{h})$. We describe the B_c-B_c' system in terms of the harmonic-oscillator eigenfunction $\psi_{nl}(\mathbf{h})$ in the momentum representation, where n denotes the principal quantum number of the system. Thus, $\Psi^B(\mathbf{h})$ is given by a linear combination of $\psi_{nl}(\mathbf{h})$. Using a parameter R_0 which represents an average separation between B_c and B_c', $\psi_{nl}(\mathbf{h})$ is written as

$$\psi_{nl}(\mathbf{h})=N_{nl}R_0{}^{3/2}Y_l(\hat{\mathbf{h}})(R_0h)^l f_{nl}(R_0{}^2h^2)e^{-R_0{}^2h^2/2}, \tag{3.1}$$

where $\hat{\mathbf{h}}=\mathbf{h}/h$, $Y_l(\hat{\mathbf{h}})$ is the normalized spherical harmonics, $f_{nl}(x)$ is the polynomial of x, and N_{nl} is the normalization constant. Throughout this paper, the magnetic quantum number is omitted.

According to the scheme (A), the effective interaction $V_\pi(nl)$ for $\psi_{nl}(\mathbf{h})$ is the product of three factors:

$$V_\pi(nl)=(2\pi)^3\delta^3(\mathbf{h}'+\mathbf{q}-\mathbf{h})\chi_n H_\pi(\mathbf{q})g_{nl}(\mathbf{h}',\mathbf{h}) . \tag{3.2}$$

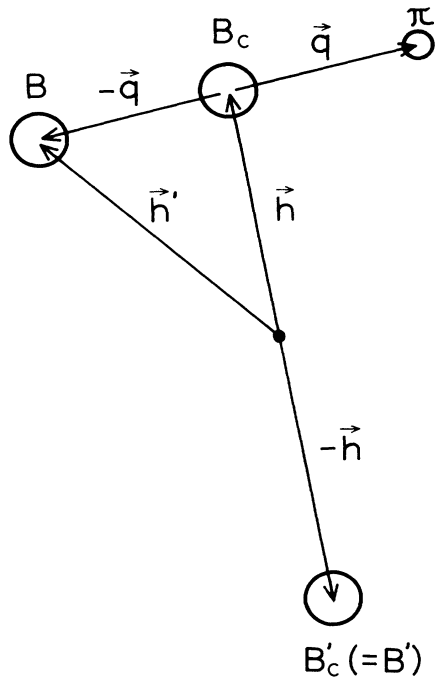

FIG. 3. The relation of the momenta.

The factor $g_{nl}(\mathbf{h}',\mathbf{h})$ represents the transformation of the q^6 system, $H_\pi(\mathbf{q})$ is the interaction term of the pion production from a baryon cluster, and χ_n is the factor representing the enhancement of the baryonic component Ψ^B in the q^6 wave function due to the system transformation before pion emission.

A. $g_{nl}(\mathbf{h}',\mathbf{h})$

This factor reflects the increase in the B_c-B_c' separation accompanying the transformation of the system. Here we assume this system transformation to be adiabatic as a first approximation, when the disturbance caused by the recoil of the pion emission is neglected, which can be described by increasing the separation parameter: $R_0 \to R_1$. Calculating the operator which change the parameter R_0 to R_1 in (3.1) and approximating $\mathbf{h}'$ by $\mathbf{h}$ in the soft-pion production, one obtains

$$g_{nl}(\mathbf{h},\mathbf{h}) = \left[\frac{R_1}{R_0}\right]^{l+3/2} e^{-R_\pi^2 h^2/2} f_{nl}(R_1^2 h^2)/f_{nl}(R_0^2 h^2) , \tag{3.3}$$

where $R_\pi = (R_1^2 - R_0^2)^{1/2}$. Hereafter, we adopt R_π as a free parameter which represents the transformation of the system.

According to QCD, the quarks in a hadronic system are enveloped by glue (gluon) and the shock of the pion emission is not transmitted from B_c to B_c', and only B_c takes part in the continued system transformation leaving B_c' as a spectator. This means that the momentum $\mathbf{h}'$ of B_c should be used to describe the system transformation after the pion emission, while $\mathbf{h}$ is used before pion emission.

Next, we derive an approximate expression for $g_{nl}(\mathbf{h}',\mathbf{h})$ by modifying two factors $e^{-R_\pi^2 h^2/2}$ and $f_{nl}(R_1^2 h^2)$ in (3.3). Considering that a pion is emitted in the midst of a transformation, we simply assume that the first factor $e^{-R_\pi^2 h^2/2}$ reduces to the symmetric form $e^{-R_\pi^2(h'^2+h^2)/4}$. This implies that the system transformation before and after the pion emission is described approximately by the successive variations of the separation parameter $R_0 \to R_m$ and $R_m \to R_1$, respectively, where

$$R_m = (R_0^2 + R_\pi^2/2)^{1/2}, \quad R_1 = (R_0^2 + R_\pi^2)^{1/2} . \tag{3.4}$$

Since the system transformation after the pion emission may still keep some adiabatic properties, this assumption appears to be reasonable.

We modify the second factor $f_{nl}(R_1^2 h^2)$ by correcting the argument $R_1^2 h^2$ according to the above two successive parameter variations, i.e., the modified factor is taken to be

$$f_{nl}((R_1^2 - R_m^2)h'^2 + R_m^2 h^2) .$$

Then, $g_{nl}(\mathbf{h}',\mathbf{h})$ is written as

$$g_{nl}(\mathbf{h}',\mathbf{h}) = \left[\frac{R_1}{R_0}\right]^{l+3/2} \zeta(h')\zeta(h) f_{nl}((R_1^2 - R_m^2)h'^2 + R_m^2 h^2)/f_{nl}(R_0^2 h^2) , \tag{3.5}$$

where

$$\zeta(h) = e^{-R_\pi^2 h^2/4} . \tag{3.6}$$

B. $H_\pi(\mathbf{q})$

Here we adopt the following P-wave πqq interaction and derive the pion-emission interaction $H_\pi(\mathbf{q})$ by operating with it on each quark in the baryon cluster:

$$\frac{f_0}{m_\pi \sqrt{2q_0}} (\boldsymbol{\sigma}\cdot\mathbf{q})\boldsymbol{\tau} , \tag{3.7}$$

where $\boldsymbol{\sigma}$ and $\boldsymbol{\tau}$ are the spin and isospin matrix of the quark, respectively, q_0 is the energy of the emitted pion, f_0 is the coupling constant, and m_π is the pion rest mass. The calculation is straightforward and the result is

$$H_\pi(\mathbf{q}) = \sqrt{4\pi}\frac{q}{m_\pi}\frac{\sqrt{3} f_{\pi NN}}{\sqrt{2q_0}} \left[P(N_c \to \pi N_c) + \frac{2\sqrt{2}}{5} P(\Delta_c \to \pi N_c) + \cdots \right] , \tag{3.8}$$

$$f_{\pi NN} = \tfrac{5}{3} f_0 , \tag{3.9}$$

where $f_{\pi NN}$ is the coupling constant of the P-wave $\pi N_c N_c$ interaction and $P(N_c \to \pi N_c)[P(\Delta_c \to \pi N_c)]$ is the operator which changes the N_c (N-cluster) [Δ_c] state to the P-wave πN_c state. The recoil of N_c [Δ_c] in pion emission is neglected. Although the $\pi B_c B_c'$ interaction generally accompanies the form factor caused by the expansion of B_c, this is omitted in formula (3.8). This point will be discussed further. Strictly speaking the $f_{\pi NN}$ must be different from the coupling constant of a system of a "real" nucleon and a pion. In the present analysis, however, we identify the baryon cluster B_c with the real baryon B and use the empirical πNN coupling constant in place of the $f_{\pi NN}$, i.e.,

$$\frac{f_{\pi NN}{}^2}{4\pi} \sim 0.08 \ . \tag{3.10}$$

C. χ_n

In the diquark-cluster model, the mass spectrum of the dibaryon is originally given by

$$M_0 = 6m + n\omega \ . \tag{3.11}$$

The difference Δ between the mass M of an actual $1p\frac{1}{2}$-shell dibaryon and M_0 is caused by the strong LS force in the q^6 system. With the parameters given in Sec. II, Δ is estimated to be

$$\Delta = \begin{cases} 260 \text{ MeV} & \text{for } n=2 \ \ [B_1^2(2.14)2^+] \ , \\ 450 \text{ MeV} & \text{for } n=3 \ \ [B_1^2(2.22)3^-] \ . \end{cases} \tag{3.12}$$

Since the LS force between two real nucleons is rather weak, it is inferred that the LS force between two baryon clusters is also weak and the energy for the baryonic component Ψ^B in the q^6 wave function Ψ is given by (3.11) as a first approximation.

In the description of (A), it is assumed that the system transformation occurs easily for the baryonic component Ψ^B and the effective separation parameter R^{eff} may be close to R_m which is considerably larger than R_0. Upon an increase in separation, the excitation energy ω may diminish to ω', and formula (3.11) becomes

$$M_0' = 6m + n\omega z \ , \tag{3.13}$$

where the parameter z (<1) is

$$z = \frac{\omega'}{\omega} \ . \tag{3.14}$$

In the diquark-cluster model, the baryonic component Ψ^B occupies a small portion of the q^6 wave function, i.e., only a few percentage points in probability. However this small component Ψ^B is enhanced by the above-mentioned energy reduction because generally the amplitude of a small component in a state is inversely proportional to the difference between the proper energy of the component and state energy as a first approximation. The enhancing factor χ_n reflects this mechanism and is given by the ratio of the energy difference

$$\chi_n = \frac{M_0 - M}{M_0' - M} \ .$$

This can be written as

$$\chi_n = \frac{\kappa}{\kappa - 1 + z} \ , \tag{3.15}$$

where

$$\kappa = \frac{\Delta}{n\omega} = \begin{cases} 0.43 & \text{for } n=2 \ , \\ 0.50 & \text{for } n=3 \ . \end{cases} \tag{3.16}$$

With $z=0.7$, for example, one obtains enhancing factors that are quite large:

$$\chi_2 = 3.2, \quad \chi_3 = 2.5 \ . \tag{3.17}$$

Of course, formula (3.15) can be used only if the mixing probability $|\chi_n \Psi^B|^2$ is smaller than unity.

Note that the strong enhancement of the amplitude by the above mechanism may not occur in the baryonic components involving internally excited baryons with $n=1$. As pointed out by Isgur and Karl,[30] the energy for the P-wave excitation of the baryon is unusually large (~ 520 MeV) compared with ω (~ 300 MeV). This indicates that the energy of the system is shifted higher by ~ 220 MeV resulting in the strong reduction of χ_n. In fact with this modification (3.17) becomes

$$\chi_2 = 0.87, \quad \chi_3 = 1.13 \ . \tag{3.18}$$

IV. CALCULATION OF PARTIAL DECAY WIDTHS

In this section we outline our calculation of the partial decay widths $\Gamma^{\pi NN}$, $\Gamma^{\pi d}$, and Γ^{NN} based on the diquark-cluster model and decay dynamics presented in the previous section.

The following approach is adopted in the calculation of the matrix elements.

(1) The wave function of the system is completely antisymmetrized with respect to the color, flavor, spin, and space coordinates of constituent six quarks.

(2) The Born approximation involving the $^3S_1$ NN final-state interaction is adopted.

(3) Complete partial-wave expansion is carried out to calculate each partial amplitude precisely, involving the effects of the interference among various processes.

First of all we consider a system which consists of two baryons with relative momentum $\mathbf{k}$ and a pion with momentum $\mathbf{q}$ in the c.m. system. We assume that the first baryon B and the second baryon B' involve quarks q_1, q_2, q_3 and q_4, q_5, q_6, respectively. We write the wave function as

$$\Psi^p(123,456) = \Phi(123,456) e^{i\mathbf{k}\cdot\mathbf{r} + i\mathbf{q}\cdot\mathbf{r}_\pi} \ , \tag{4.1}$$

where $\mathbf{r}$ is the separation between the two baryons, $\mathbf{r}_\pi$ is the separation of the pion from the center of the two baryons, and $\Phi(123,456)$ describes the color, isospin, and spin states of the system as well as the internal motions of the quarks in the baryons. We antisymmetrize and normalize $\Phi(123,456)$ for both of the subsets (q_1,q_2,q_3) and (q_4,q_5,q_6):

$$|\Phi(123,456)|^2 = 1 \ . \tag{4.2}$$

The full wave function Ψ^F of this two-baryon system is

obtained by the antisymmetrization of $\Psi^P(123,456)$:

$$\Psi^F = N_F \sum (-) \Psi^P(123,456) , \tag{4.3}$$

where the summation runs over the set of all possible partitions of the six quarks into two subsets of three quarks each. The factor $(-)$ is $+1$ for even permutations and -1 for odd ones. As a first approximation each of ten terms in (4.3) is orthogonal to the others, so that the normalization constant N_F is

$$N_F = \frac{1}{\sqrt{10}} . \tag{4.4}$$

Adopting the Born approximation, the matrix element $\mathcal{M}_\pi$ for the production of one pion can written as

$$\mathcal{M}_\pi = \langle \Psi^F | V_\pi | \Psi \rangle , \tag{4.5}$$

where V_π operates on all possible baryon clusters in Ψ^B. Because the q^6 wave function Ψ is antisymmetrical with respect to the constituent six quarks, each of the ten terms in (4.3) contributes equally to $\mathcal{M}_\pi$ in (4.5). Therefore (4.5) becomes

$$\mathcal{M}_\pi = \sqrt{10} \langle \Psi^p(123,456) | V_\pi | \Psi \rangle . \tag{4.6}$$

In the following scheme we present the calculation of the matrix element $\mathcal{M}_\pi$.

A. q^6 wave function Ψ

As stated in Sec. II, within the quark shell model with the *jj*-coupling scheme, we assume the form for the harmonic-oscillator wave function. The full wave function can be written as

$$\Psi = N_a \sum (-) N_s \Phi^{JJ} r_1^{\,l_1} r_2^{\,l_2} \cdots r_6^{\,l_6} e^{-(r_1^2+r_2^2+\cdots+r_6^2)/2R^2} , \tag{4.7}$$

where

$$R = \frac{1}{\sqrt{m\omega}} , \tag{4.8}$$

and $\mathbf{r}_i$ represents the distance of the ith quark q_i and its origin, Φ^{JJ} is a normalized color-isospin-spin-angular wave function within the *jj*-coupling scheme, N_s and N_a are the normalization constants for a single term and full wave function, respectively, l_i the orbital angular momentum of q_i, and the summation runs over all possible permutation of the constituent six quarks. For simplicity we assume that none of six quarks is radially excited. The maximum orbital momentum L in the system is then given by

$$L = l_1 + l_2 + \cdots + l_6 . \tag{4.9}$$

B. Extraction of the effective component Ψ^{eff} from Ψ

Among the various components of Ψ in (4.7), only the baryonic component Ψ^B in which (q_1,q_2,q_3) form a baryon cluster B_c and (q_4,q_5,q_6) form the other cluster B_c', provides a nonvanishing contribution in (4.6). To discuss this we introduce a new coordinate system $(\boldsymbol{\zeta},\mathbf{r},\mathbf{s}_1,\mathbf{s}_2,\mathbf{t}_1,\mathbf{t}_2)$, illustrated in Fig. 4, where $\mathbf{r}_i$ is given by

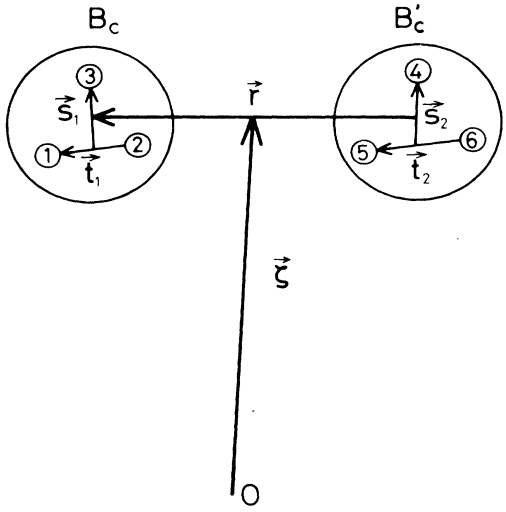

FIG. 4. Coordinate system for q^6 system.

$$\begin{aligned}
\mathbf{r}_1 &= \boldsymbol{\zeta} + \tfrac{1}{2}\mathbf{r} - \tfrac{1}{3}\mathbf{s}_1 + \tfrac{1}{2}\mathbf{t}_1 , \\
\mathbf{r}_2 &= \boldsymbol{\zeta} + \tfrac{1}{2}\mathbf{r} - \tfrac{1}{3}\mathbf{s}_1 - \tfrac{1}{2}\mathbf{t}_1 , \\
\mathbf{r}_3 &= \boldsymbol{\zeta} + \tfrac{1}{2}\mathbf{r} + \tfrac{2}{3}\mathbf{s}_1 , \\
\mathbf{r}_4 &= \boldsymbol{\zeta} - \tfrac{1}{2}\mathbf{r} + \tfrac{2}{3}\mathbf{s}_2 , \\
\mathbf{r}_5 &= \boldsymbol{\zeta} - \tfrac{1}{2}\mathbf{r} - \tfrac{1}{3}\mathbf{s}_2 + \tfrac{1}{2}\mathbf{t}_2 , \\
\mathbf{r}_6 &= \boldsymbol{\zeta} - \tfrac{1}{2}\mathbf{r} - \tfrac{1}{3}\mathbf{s}_2 - \tfrac{1}{2}\mathbf{t}_2 .
\end{aligned} \tag{4.10}$$

With these variables, one can write

$$\sum_i r_i^2 = 6\zeta^2 + \tfrac{3}{2}r^2 + \tfrac{2}{3}(s_1^2+s_2^2) + \tfrac{1}{2}(t_1^2+t_2^2) . \tag{4.11}$$

The factor $\Phi^{JJ} r_1^{\,l_1} r_2^{\,l_2} \cdots r_6^{\,l_6}$ in (4.7) is a polynomial of $\mathbf{r}_i$ and, among the components of $\mathbf{r}_i$, only the vector $\mathbf{r}$ is responsible for the excitation of the two-baryon system. Therefore, we can extract the effective component Ψ^{eff} from Ψ by the following simple substitution in $\Phi^{JJ} r_1^{\,l_1} r_2^{\,l_2} \cdots r_6^{\,l_6}$:

$$\mathbf{r}_1, \mathbf{r}_2, \mathbf{r}_3 \to \tfrac{1}{2}\mathbf{r}, \quad \mathbf{r}_4, \mathbf{r}_5, \mathbf{r}_6 \to -\tfrac{1}{2}\mathbf{r} . \tag{4.12}$$

The result can be written as

$$\Psi^{\text{eff}} = N_a \sum (-)(-1)^{\tilde{L}} (4\pi)^{5/2} 6^{-L/2} C_g \Phi^{JJ}(\hat{\mathbf{r}}) N_{LL} R_0^{-3/2} \left[\frac{r}{R_0}\right]^L e^{-r^2/2R_0^2} \psi^I , \tag{4.13}$$

where

$$R_0=(\tfrac{2}{3})^{1/2}R\ , \tag{4.14}$$

$$\tilde{L}=l_4+l_5+l_6\ , \tag{4.15}$$

$$C_g=\left[\frac{[\Gamma(\frac{3}{2})]^5\Gamma(L+\frac{3}{2})}{\Gamma(l_1+\frac{3}{2})\Gamma(l_2+\frac{3}{2})\cdots\Gamma(l_6+\frac{3}{2})}\right]^{1/2}\ , \tag{4.16}$$

$$\psi^I=N_I e^{-[6\xi^2+2/3(s_1{}^2+s_2{}^2)+1/2(t_1{}^2+t_2{}^2)]/2R^2}\ , \tag{4.17}$$

and $\Phi^{JJ}(\hat{\mathbf{r}})$ is the function of $\hat{\mathbf{r}}$ obtained by substituting $\hat{\mathbf{r}}$ for $\hat{\mathbf{r}}_i$ in Φ^{JJ}. The wave function ψ^I with the normalization constant N_I describes the spurious motion of the center of mass as well as the states of quarks inside the baryons.

C. Extraction of Ψ^B from $\Psi^{\rm eff}$ with partial-wave expansion

Next we carry out the partial-wave expansion of $\Psi^{\rm eff}$ in terms of the eigenfunctions of the harmonic oscillator B_c-B_c'. The eigenfunctions can be written as

$$\Phi^{BB'}(IlSJ:\hat{\mathbf{r}})f_{nl}(r^2/R_0{}^2)\left[\frac{r}{R_0}\right]^l e^{-r^2/2R_0{}^2}\psi^I\ .$$

Here $\Phi^{BB'}(IlSJ:\hat{\mathbf{r}})$ represents the color-isospin-spin-angular wave function of the B_c-B_c' system with an isospin I, orbital angular momentum l, spin S, and total angular momentum J within an LS-coupling scheme. The nonbaryonic components of $\Psi^{\rm eff}$ are automatically eliminated in this procedure, and $\Psi^{\rm eff}$ becomes the baryonic component Ψ^B. Taking the Fourier transform with respect to the relative momentum $\mathbf{h}$ of B_c-B_c', the momentum representation $\Psi^B(\mathbf{h})$ can be obtained. The result is

$$\Psi^B(\mathbf{h})=(2\pi)^{3/2}6^{-L/2}\sum_l(-i)^l N_{Ll}R_0{}^{3/2}f_{Ll}(R_0{}^2h^2)(R_0h)^l e^{-R_0{}^2h^2/2}\sum_s\sum_{B,B'}\epsilon^{BB'}(LlS)\Phi^{BB'}(IlSJ:\hat{\mathbf{h}})\psi^I\ , \tag{4.18}$$

where the summation with respect to B,B' runs over two baryonic cluster states N_c and Δ_c (the subscript c is omitted for simplicity). The decay strength parameter $\epsilon^{BB'}(nlS)$ is given by

$$\epsilon^{BB'}(nlS)=(-i)^{n-l}C_g N_{LL}N_{nl}{}^{-1}a_{nlL}Z^{BB'}(lS)\ , \tag{4.19}$$

where a_{nlL} is the coefficient of expansion

$$X^{(L-l)/2}=\sum_n a_{nlL}f_{nl}(X) \tag{4.20}$$

and

$$Z^{BB'}(lS)=(4\pi)^{5/2}N_a\sum(-)(-1)^{\tilde{L}}\int[\Phi^{BB'}(IlSJ:\mathbf{r})]^\dagger\Phi^{JJ}(\hat{\mathbf{r}})d\Omega_r\ . \tag{4.21}$$

In Appendix A we tabulate the values for $\epsilon^{BB'}(LlS)$ for low-lying $1p\frac{1}{2}$-shell dibaryons. Note that, in Eq. (4.18), there is no contribution from states with $n\neq L$. This is because none of the six quarks in ψ are radially excited. We also note that the separation parameter R_0 in (3.1) is given by (4.14).

D. Approximation

The matrix (4.6) can be written as

$$\mathcal{M}_\pi=\sqrt{10}\langle\Psi^p(123,456)\,|\,V_\pi\,|\,\psi^B\rangle$$

and expression (4.1) shows that this formula involves the integration with respect to variables $\mathbf{r}$ and $\mathbf{r}_\pi$. When this integration is performed for $V_\pi\,|\,\Psi^B\rangle$, it becomes the momentum representation $V_\pi\Psi^B(\mathbf{h})$, in which two momenta $\mathbf{h}$ and $\mathbf{h}'$ are

$$\begin{aligned}&\mathbf{h}=\mathbf{k}+\tfrac{1}{2}\mathbf{q}\\ &\mathbf{h}'=\mathbf{k}-\tfrac{1}{2}\mathbf{q}\end{aligned}\ \Big|\ \begin{aligned}&\text{for the case in which } B_c\\ &\text{emits a pion}\\ &\text{(as illustrated in Fig. 3)}\ ,\end{aligned}$$

$$\begin{aligned}&\mathbf{h}=\mathbf{k}-\tfrac{1}{2}\mathbf{q}\\ &\mathbf{h}'=-\mathbf{k}-\tfrac{1}{2}\mathbf{q}\end{aligned}\ \Big|\ \begin{aligned}&\text{for the case in which } B_c'\\ &\text{emits a pion}\ .\end{aligned} \tag{4.22}$$

The matrix element (4.6) is expressed as a function of the isospin and spin coordinates of the two nucleons in the final state and momenta $\mathbf{k}$ and $\mathbf{q}$. The matrix element for the transition to each πNN channels is constructed with this function. This procedure is equivalent to the partial-wave expansion of $V_\pi\Psi^B(\mathbf{h})$ for the final πNN state, and the matrix elements are given by the coefficients of the

series. Operating with V_π on $\Psi^B(\mathbf{h})$, each term in (4.18) is multiplied by $V_\pi(Ll)$ as it is a linear combination of $\psi_{nl}(\mathbf{h})$. Then each term of $V_\pi\Psi^B(\mathbf{h})$ involves the factor

$$g_{Ll}(\mathbf{h}',\mathbf{h})f_{Ll}(R_0{}^2h^2)e^{-R_0{}^2h^2/2} .$$

Using expression (3.5) and Eq. (3.4), this factor is approximately

$$\sim f_{Ll}(X)e^{-X/2} , \tag{4.23}$$

where

$$X=\frac{R_1{}^2(h'^2+h^2)}{2}-\frac{R_0{}^2(h'^2-h^2)}{2} . \tag{4.24}$$

Using (4.22), one obtains

$$X=R_1{}^2\left[k^2+\left[\frac{q}{2}\right]^2\right]\pm R_0{}^2\mathbf{k}\cdot\mathbf{q} .$$

In the case $R_0{}^2/R_1{}^2\ll 1$, the second term can be neglected and

$$X\sim R_1{}^2\left[k^2+\left[\frac{q}{2}\right]^2\right] . \tag{4.25}$$

Since all of the arguments in the exponential function in $V_\pi\Psi^B(\mathbf{h})$ become independent of the angle between $\mathbf{k}$ and $\mathbf{q}$, with this approximation, the partial-wave expansion of $V_\pi\Psi^B(\mathbf{h})$ can easily be performed. As will be shown in Sec. VI the actual value of $R_0{}^2/R_1{}^2$ is sufficiently small (~ 0.07) so that the error caused by this approximation is negligible. For this reason, we hereafter adopt the approximation (4.25).

E. Matrix elements for $q^6\to\pi NN$ transition without NN final-state interaction

The matrix elements $m(l_kl_ql_tS_k)$ for $q^6\to\pi NN$ transition are given by the coefficients in the partial-wave expansion of $V_\pi\Psi^B(\mathbf{h})$ using the normalized color-isospin-spin-angular πNN wave function $\Phi^{NN}(Il_kl_ql_tS_kJ:\hat{\mathbf{k}},\hat{\mathbf{q}})$ for the exit channel. The terms l_k and l_q represent the orbital angular momenta of the NN subsystem and of the pion in the c.m. system. The total angular momentum of l_k and l_q is l_t, the total spin is S_k. The NN final-state interaction is not taken into account in this step. The result is given by

$$m(l_kl_ql_tS_k)=(2\pi)^2\sqrt{10}\,6^{-L/2}\frac{q}{m_\pi}\frac{\sqrt{3}f_{\pi NN}}{\sqrt{q_0}}R_1{}^{3/2}e^{-X/2}e^{-R_0{}^2q^2/2}H(l_kl_ql_tS_k:k,q) , \tag{4.26}$$

where

$$H(l_kl_ql_tS_k:k,q)=2\sum(-i)^lN_{Ll}\chi_Lf_{Ll}(X)G(l_kl_ql_tS_k,Ll;k,q) , \tag{4.27}$$

$$G(l_kl_ql_tS_k,Ll:k,q)=\sum_s\left[\epsilon^{NN}(LlS)F^{NN}(l_kl_ql_tS_k,lS:k,q)+\frac{2\sqrt{2}}{5}\epsilon^{N\Delta}(LlS)F^{N\Delta}(l_kl_ql_tS_k,lS:k,q)\right] , \tag{4.28}$$

$$F^{NB}(l_kl_ql_tS_k,lS:k,q)=\int\int d\Omega_kd\Omega_q(R_1h)^l[\Phi^{NN}(Il_kl_ql_tS_kJ:\hat{\mathbf{k}},\hat{\mathbf{q}})]^\dagger P(B_c\to\pi N_c)\Phi^{NB}(IlSJ:\hat{\mathbf{h}}) , \tag{4.29}$$

and X is given by (4.25). In Eq. (4.26), the factor $e^{-R_0{}^2q^2/2}$ represents a form factor which is related to the emission of a pion from a quark in the baryon cluster and is calculated with the use of the baryon cluster wave function in (4.17).

Since the factor $h^l\phi^{NB}(IlSJ:\mathbf{h})$ is a polynomial of $\mathbf{h}(=\mathbf{k}+\frac{1}{2}\mathbf{q})$, the formula (4.29) can be written as

$$F^{NB}(l_kl_ql_tS_k,lS:k,q)=(R_1k)^{l_k}\left[R_1\frac{q}{2}\right]^{l-l_k}A^{NB}(l_kl_ql_tS_k:lS) , \tag{4.30}$$

where $A^{NB}(l_kl_ql_tS_k:lS)$ is a constant. It should be noted that $F^{NB}(l_kl_ql_tS_k,lS:k,q)$ vanishes outside the range

$$0\le l_k\le l,\quad l_q=l-l_k\pm 1 , \tag{4.31}$$

and this simplifies the calculation. The values for $A^{NB}(l_kl_ql_tS_k:lS)$ for the low-lying $1p\frac{1}{2}$-shell dibaryon are tabulated in Appendix B.

F. Inclusion of the NN final-state interaction

The $q^6\to\pi NN$ transition with $l_k=0$ and $S_k=1$ is influenced by the strong ${}^3S_1$ NN final-state interaction. We take this effect into account simply by subtracting the deuteron component from matrix element $m(0l_ql_q1)$ given in (4.26). Specifically, for the factor $H(0l_ql_q1:k,q)e^{-R_1{}^2k^2/2}$, we perform the substitution

$$H(0l_ql_q1:k,q)e^{-R_1{}^2k^2/2}\to H(0l_ql_q1:k,q)e^{-R_1{}^2k^2/2}-\frac{1}{(2\pi R_1)^{3/2}}\phi_s(k)H_d(l_q:q) , \tag{4.32}$$

where

$$H_d(l_q:q)=\frac{{R_1}^{3/2}}{(2\pi)^{3/2}}\int_0^\infty \phi_s^*(k)e^{-{R_1}^2k^2/2}H(0l_ql_q1:k,q)k^2dk \tag{4.33}$$

and $\phi_s(k)$ represents the S-wave component of the deuteron wave function in the momentum representation and is normalized as

$$\frac{1}{(2\pi)^3}\int_0^\infty |\phi_s(k)|^2k^2dk=1 . \tag{4.34}$$

In this paper $\phi_s(k)$ is taken to be

$$\phi_s(k)=N_d\left[\frac{1}{k^2+\gamma^2}-\frac{1}{k^2+\beta^2}\right],\quad N_d=(2\pi)^{3/2}\left[\frac{4\gamma\beta(\beta+\gamma)}{\pi(\beta-\gamma)^2}\right]^{1/2},\quad \gamma=\sqrt{m_NB} , \tag{4.35}$$

where m_N and B represent the nucleon mass and deuteron binding energy, respectively, and the parameter β is taken as $\beta=5.87\gamma$.

G. Matrix elements for the $q^6\to\pi d$ transition

In the dibaryon with $I=1$, a transition to the πd channel can also occur. Neglecting the contribution from the D-wave component of the deuteron wave function, the matrix element $m_d(l_q)$ for the $q^6\to\pi d$ transition is given by

$$m_d(l_q)=\frac{1}{(2\pi)^3}\int_0^\infty \phi_s^*(k)m(0l_ql_q1)k^2dk . \tag{4.36}$$

Using (4.26) this can be written as

$$m_d(l_q)=\sqrt{2\pi}\sqrt{10}\,6^{-L/2}\frac{q}{m_\pi}\frac{\sqrt{3}f_{\pi NN}}{q_0}e^{-R_0^2q^2/2}e^{-{R_1}^2(q/2)^2/2}H_d(l_q:q) . \tag{4.37}$$

H. Matrix element for the $q^6\to NN$ transition

In this section we discuss the $q^6\to NN$ transition. As previously stated, this process is not a direct transition but is caused by the reabsorption of the pion into the baryon B which is produced by the transition $q^6\to\pi NB$. The Feynman diagrams for this process are illustrated in Figs. 5(a) and 5(b). The first diagram (a) in Fig. 5 is of a self-energy type which involves two intermediate states: πN and $\pi\Delta$. The contribution from these intermediate states to the matrix element can be written by the one factor V_N which is independent of the isospin and spin states of the system.

$$\begin{aligned}V_N=-\frac{3{f_{\pi NN}}^2\xi(h)\chi_n}{2{m_\pi}^2}\left[\frac{R_1}{R_0}\right]^{l+3/2}&\frac{1}{(2\pi)^3}\int d^3q\frac{q^2}{q^0}e^{-R_0^2q^2/2}e^{-{R_\pi}^2(\mathbf{h}-\mathbf{q})^2/4}\\&\times\left[\frac{1}{q_0+[(\mathbf{h}-\mathbf{q})^2+{m_N}^2]^{1/2}-(h^2+{m_N}^2)^{1/2}}\right.\\&\left.+\frac{32}{25}\frac{1}{q_0+[(\mathbf{h}-\mathbf{q})^2+{m_\Delta}^2]^{1/2}-(h^2+{m_N}^2)^{1/2}}\right]\\&\times f_{LI}(({R_1}^2-{R_m}^2)(h-q)^2+{R_m}^2h^2) .\end{aligned} \tag{4.38}$$

Since the value of h is much larger than ${R_\pi}^{-1}$ and m_π in the integrand, for the terms that do not appear in the arguments of the exponential functions, we make the approximations

$$\mathbf{q}\sim\mathbf{h},\quad q_0\sim h .$$

In this manner V_N can be written as

$$V_N=V_0\xi(h)e^{-uR_0^2h^2/2}\left[\frac{R_1}{R_0}\right]^{l+3/2}\chi_Lf_{LI}({R_m}^2h^2/2) , \tag{4.39}$$

where

$$V_0=-\frac{6}{\sqrt{\pi}}\frac{f_{\pi NN}{}^2}{4\pi}\frac{1}{(R_2 m_\pi)^2}\frac{1}{R_2}\left[\left[1-\frac{h}{(h^2+m_N{}^2)^{1/2}+m_N}\right]^{-1}+\frac{32}{25}\left[1-\frac{h}{(h^2+m_N{}^2)^{1/2}+m_N}+\frac{m_\Delta-m_N}{h}\right]^{-1}\right] \tag{4.40}$$

and

$$R_2=(R_\pi{}^2+2R_0{}^2)^{1/2},\quad u=(R_\pi/R_2)^2\ . \tag{4.41}$$

Using (4.39) the matrix element $m_N^{\rm sel}(l_k)$ in the first diagram in Fig. 5 can be written as

$$m_N^{\rm sel}(l_k)=2(2\pi)^{3/2}\sqrt{10}\,6^{-L/2}(-i)^l R_1^{l+3/2}V_0\xi(h)\chi_L N_{Ll}\epsilon^{NN}(LlS)f_{Ll}(R_m{}^2h^2)h^l e^{-(1+u)R_0{}^2h^2/2}\ , \tag{4.42}$$

where $l=l_k$.

The second diagram in Fig. 5 is of a vertex type which involves a one-pion-exchange potential. According to process (A), the two baryon clusters in the transformed q^6 system are quite separate from each other when the fission of the system takes place. Therefore, the matrix element $m_N^{\rm ex}(l_k)$ for the process (b) may be negligible in magnitude, except in the special case when $l=0$ (separation between the two baryon clusters is relatively small when the system is in the S state). Discarding the contributions from the $l\neq 0$ states and using the same approximation as in $m_N^{\rm sel}(l_k)$, one obtains

$$m_N^{\rm ex}(l_k)=2(2\pi)^{3/2}\sqrt{10}\,6^{-L/2}(u'R_1)^{3/2}V_0\xi(h)\chi_L N_{L0}B(l_k)f_{L0}((R_1{}^2-R_m{}^2)h^2)e^{-u'R_0{}^2h^2/2}\ , \tag{4.43}$$

where

$$R_4=\sqrt{R_\pi{}^2+4R_0{}^2},\quad u'=(R_2/R_4)^2\ , \tag{4.44}$$

and $B(l_k)$ represents the kinematic constants which are given below.

For $I=1$ and $J^p=2^+$

$$B(0)=0,\quad B(2)=\tfrac{16}{15}(\tfrac{2}{5})^{1/2}\epsilon^{N\Delta}(202)-\tfrac{16}{75}\epsilon^{\Delta\Delta}(202)\ . \tag{4.45}$$

For $I=1$ and $J^p=0^+$

$$B(0)=-\frac{1}{3}\epsilon^{NN}(200)+\frac{16}{15\sqrt{5}}\epsilon^{\Delta\Delta}(200),\quad B(2)=0\ .$$

For $I=0$ and $J^p=1^+$

$$B(0)=-\frac{1}{3}\epsilon^{NN}(201)+\frac{16}{15\sqrt{5}}\epsilon^{\Delta\Delta}(201),\quad B(2)=-\frac{2\sqrt{2}}{3}\epsilon^{NN}(201)+\frac{16\sqrt{2}}{75\sqrt{5}}\epsilon^{\Delta\Delta}(201)\ . \tag{4.46}$$

The total matrix element $m_N(l_k)$ is given by

$$m_N(l_k)=m_N^{\rm sel}(l_k)+m_N^{\rm ex}(l_k)\ . \tag{4.47}$$

I. Calculation of the partial decay widths

The calculation of the partial decay widths is straightforward. We define the partial widths and total width at total energy E by

$$\Gamma^{\pi NN}(E)=\sum\Gamma^{\pi NN}(l_k l_q l_t S_k{:}E)\ , \tag{4.48}$$

$$\Gamma^{\pi NN}(l_k l_q l_t S_k{:}E)=\frac{1}{(2\pi)^6}\int\int 2\pi\delta\left[E-2m_N-\frac{k^2}{m_N}-q_0\right]|\,m(l_k l_q l_t S_k)\,|^2 d^3q\,d^3k\ , \tag{4.49}$$

$$\Gamma^{\pi d}(E)=\sum\Gamma^{\pi d}(l_q{:}E)\ , \tag{4.50}$$

$$\Gamma^{\pi d}(l_q{:}E)=\frac{1}{(2\pi)^3}\int 2\pi\delta(E-2m_N+B-q_0)\,|\,m_d(l_q)\,|^2 d^3q\ , \tag{4.51}$$

$$\Gamma^{NN}(E)=\sum\Gamma^{NN}(l_k{:}E)\ , \tag{4.52}$$

$$\Gamma^{NN}(l_k{:}E)=\frac{1}{(2\pi)^3}\int 2\pi\delta(E-2(h^2+m_N{}^2)^{1/2})\,|\,m_N(l_k)\,|^2 d^3h\ , \tag{4.53}$$

$$\Gamma(E)=\Gamma^{\pi NN}(E)+\Gamma^{\pi d}(E)+\Gamma^{NN}(E)\ . \tag{4.54}$$

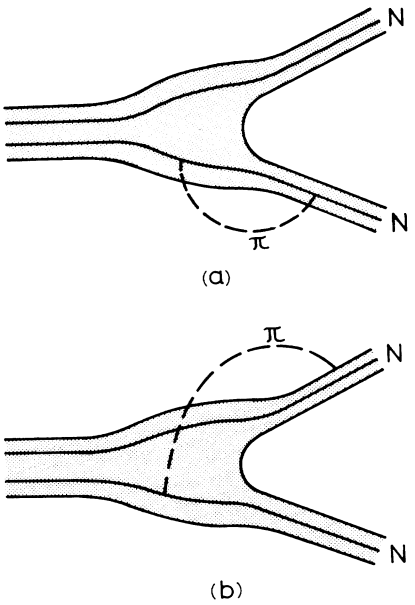

FIG. 5. The Feynman diagrams for the $q^6 \rightarrow NN$ transition. The solid lines represent three quark subsystems while the shaded region represents the gluon system.

The summation runs over all possible states.

The partial and total widths are given by

$$\Gamma^{\pi NN}=\Gamma^{\pi NN}(M)\ , \tag{4.55}$$

$$\Gamma^{\pi d}=\Gamma^{\pi d}(M)\ , \tag{4.56}$$

$$\Gamma^{NN}=\Gamma^{NN}(M)\ , \tag{4.57}$$

$$\Gamma=\Gamma^{\pi NN}+\Gamma^{\pi d}+\Gamma^{NN}\ , \tag{4.58}$$

where M represents the dibaryon rest mass.

V. CALCULATION OF THE πd AND NN PHASE SHIFTS (T MATRICES)

As shown in Table I the major dibaryons $B^2_{0,1}(2.22)3^-$ are of a single state and another major dibaryon $B^2_1(2,14)2^+$ involves two states. In the diquark-cluster model, however, many states (≥ 4) with the same quantum number degenerate to a single energy level in general. The theoretical analysis of the πd and NN phase shifts influenced by the group of these degenerate states may not be easy, because they may correlate with each other causing energy shifts and configuration mixing among them, which in turn change the phase shifts sharply. In this section we present one method for calculating the πd and NN phase shifts in such a situation.

Let ξ_i $(i=1,2,\ldots,n)$ be the n degenerate q^6 states with the same quantum number, each one orthogonal to any other. There are two principal mechanisms that cause the energy shift and configuration mixing among them. One is the coupling between ξ_i and ξ_j via the intermediate states (the πNN, πd, and NN states in the present case). The other is the residual two-body interaction, well known from nuclear-structure theory (the residual qq interaction in this case). The matrix element $M_{ij}(E)$ for the coupling between ξ_i and ξ_j at an energy E is written as

$$M_{ij}(E)=E^0_{ij}-\frac{i}{2}\Gamma_{ij}(E)\ , \tag{5.1}$$

where the imaginary part $\frac{1}{2}\Gamma_{ij}(E)$ represents the contribution from the coupling via the intermediate states. The real part of (5.1), E^0_{ij}, arises from the two-body interaction which is independent of E. The possible contributions from the virtual intermediate states are neglected simply because the estimation is very difficult. Hereafter, we use the $n\times n$ matrix representation for $M_{ij}(E)$:

$$\underline{M}(E)=[M_{ij}]=\begin{bmatrix} M_{11},M_{12},\ldots,M_{1n} \\ M_{21},M_{22},\ldots,M_{2n} \\ \cdots \\ M_{n1},M_{n2},\ldots,M_{nn} \end{bmatrix}\ , \tag{5.2}$$

where the argument E is omitted from each of the elements. E^0_{ij} and Γ_{ij} are also expressed in a matrix form:

$$\underline{E}^0=[E^0_{ij}],\quad \underline{\Gamma}(E)=[\Gamma_{ij}]\ . \tag{5.3}$$

The decay of a q^6 system is described by a set of decay strength parameters $\epsilon^{BB'}(LlS)$. For simplicity, we use a new notation ϵ_k $(k=1,2,\ldots,m)$. In $B^2_1(2.14)2^+$, for example, five decay strength parameters are employed to describe the decay and they are denoted as

$$\epsilon_1=\epsilon^{NN}(220),\quad \epsilon_2=\epsilon^{N\Delta}(221)\ ,$$

$$\epsilon_3=\epsilon^{N\Delta}(222),\quad \epsilon_4=\epsilon^{N\Delta}(202)\ ,$$

and

$$\epsilon_5=\epsilon^{\Delta\Delta}(202)\ .$$

From (4.26)–(4.28), (4.37), and (4.42)–(4.46), matrix elements depend on ϵ_k in a linear fashion. Therefore, the total decay width $\Gamma(E)$ at energy E is given by the quadratic form

$$\Gamma(E)=\sum_{k,h}\gamma_{kh}(E)\epsilon_k\epsilon_h=\mathbf{u}^{\dagger}\underline{G}(E)\mathbf{u}$$

$$[\gamma_{hk}(E)=\gamma_{kh}(E)]\ , \tag{5.4}$$

where

$$\underline{G}(E)=[\gamma_{kh}] \tag{5.5}$$

and

$$\mathbf{u}=\begin{bmatrix}\epsilon_1\\ \epsilon_2\\ \vdots\\ \epsilon_m\end{bmatrix}\ .$$

We denote the decay strength parameters for ξ_i by ϵ_{ki} and introduce a $m\times n$ matrix:

$$\underline{H}=\begin{bmatrix} \epsilon_{11},\epsilon_{12},\ldots,\epsilon_{1n} \\ \epsilon_{21},\epsilon_{22},\ldots,\epsilon_{2n} \\ \cdots \\ \epsilon_{m1},\epsilon_{m2},\ldots,\epsilon_{mn} \end{bmatrix}\ . \tag{5.6}$$

Since this matrix transforms

$$\xi_i = \begin{pmatrix} 0 \\ \vdots \\ 1 \\ \vdots \\ 0 \end{pmatrix} (i\text{th})$$

to

$$\begin{pmatrix} \epsilon_{1i} \\ \epsilon_{2i} \\ \vdots \\ \epsilon_{mi} \end{pmatrix}$$

and $\Gamma_{ii}(E)$ is the total decay width of ξ_i at energy E, it is evident that the matrix $\underline{\Gamma}(E)$ can be written as

$$\underline{\Gamma}(E)=\underline{H}^T\underline{G}(E)\underline{H} \ . \tag{5.7}$$

The actual value for $\gamma_{kh}(E)$ is easily calculated using the formula for $\Gamma(E)$ obtained in the previous section.

Concerning the residual qq interaction on E_{ij}^0, we can say only that very little is known. In this paper we evaluate them with the following assumption: a part of the color-electric interaction as well as the color-magnetic interaction still remains in the $[(1p\frac{1}{2})(1s\frac{1}{2})]$ diquarks producing energy shifts. Then, the matrix $\underline{E}^0$ becomes a function of four parameters Δ_{00}, Δ_{01}, Δ_{10}, and Δ_{11} which represent the energy shifts of the $[(1p\frac{1}{2})(1s\frac{1}{2})]$ diquarks [00], [01], [10], and [11], respectively. The possible restrictions imposed on these parameters will be discussed later. In the following we show the method for calculating the πd phase shifts using the matrix $\underline{M}(E)$.

The S matrix $\underline{S}(E)$ for the πd scattering at energy E is written as

$$\underline{S}(E)=[S_{\alpha\beta}] \ , \tag{5.8}$$

where α and β represent the states of the exit and entrance channels. For the case $l_q=J$, $\underline{s}(E)$ is composed of one element S_{11} and the phase shift is given by the relationship $S_{11}=e^{2i\delta}$. For the cases $l_q=J\pm1$, $\underline{s}(E)$ is a 2×2 matrix. It is convenient to use the T matrix $\underline{T}(E)$ defined by

$$\underline{S}(E)=\underline{I}-2\pi i\underline{T}(E) \ , \tag{5.9}$$

where $\underline{I}$ represents the unit matrix (Appendix C). The πd phase shift $\delta_{\alpha\beta}$ is commonly defined by an equation

$$-2\pi iT_{\alpha\beta}(E)=e^{2i\delta_{\alpha\beta}}-1 \ . \tag{5.10}$$

But a quite different expression is used in NN scattering as will be seen shortly.

Except for the initial- and final-state interactions, the contribution from $\{\xi_i\}$ to $\underline{T}(E)$ is given by

$$T_{\alpha\beta}(E)=\frac{1}{(2\pi)^3}\int\delta(E-2m_N+B-q_0)\left\langle\alpha\left|V_\pi\frac{1}{E-H}V_\pi^\dagger\right|\beta\right\rangle d^3q \ , \tag{5.11}$$

where H represents the total Hamiltonian for the ξ_i system (Appendix C). Inserting the identity operator $\sum_i|\xi_i\rangle\langle\xi_i|$ before and after the energy denominator, (5.11) becomes

$$T_{\alpha\beta}(E)=\frac{1}{(2\pi)^3}\int\delta(E-2m_N+B-q_0)\sum_{i,j}\langle\alpha|V_\pi|\xi_i\rangle\left\langle\xi_i\left|\frac{1}{E-H}\right|\xi_j\right\rangle\langle\xi_j|V_\pi^\dagger|\beta\rangle d^3q \ . \tag{5.12}$$

Since the Hamiltonian H can be written as $M\underline{I}+\underline{M}(E)$ in matrix representation, one obtains

$$\left\langle\xi_i\left|\frac{1}{E-H}\right|\xi_j\right\rangle=\{[(E-M)\underline{I}-\underline{M}(E)]^{-1}\}_{ij} \ . \tag{5.13}$$

In general, the matrix element for the decay of ξ_i to πd channel at energy E is a linear combination of ϵ_{ki}. Then, one can write

$$\langle\alpha|V_\pi|\xi_i\rangle=m_d(l_q)=C_{\alpha k}(E)\epsilon_{ki} \ , \tag{5.14}$$

where l_q is the orbital angular momentum of a pion in state α. Using (5.11)–(5.14), one obtains

$$\underline{T}(E)=a_d(E)\underline{C}(E)\underline{H}[(E-M)\underline{I}-\underline{M}(E)]^{-1}\underline{H}^T\underline{C}^T(E) \ , \tag{5.15}$$

where

$$\underline{C}(E)=[C_{\alpha k}] \tag{5.16}$$

and

$$a_d(E)=\frac{1}{(2\pi)^3}\int\delta(E-2m_N+B-q_0)d^3q = \frac{1}{2\pi^2}qq_0 \ . \tag{5.17}$$

It should be noted that the partial decay width $\Gamma^{\pi d}(l_q{:}E)$ of ξ_i is given by $2\pi a_d(E)\,|\,[\underline{C}(E)\underline{H}]_{\alpha i}\,|^2$.

The T matrix in NN scattering is obtained in almost the same manner. The factor $a_d(E)$ in (5.15) should be replaced by

$$a_N(E)=\frac{1}{(2\pi)^3}\int\delta(E-2(h^2+m_N{}^2)^{1/2})d^3h = \frac{1}{4\pi^2}h(h^2+m_N{}^2)^{1/2} \ . \tag{5.18}$$

It is noted that in NN scattering, using two phase shifts $\delta_1(E)$ and $\delta_2(E)$ and one mixing parameter $\epsilon(E)$, the S matrix is commonly written as

$$\underline{S}(E)=\begin{pmatrix} e^{2i\delta_1}\cos(2\epsilon) & e^{i(\delta_1+\delta_2)}\sin(2\epsilon) \\ e^{i(\delta_1+\delta_2)}\sin(2\epsilon) & e^{2i\delta_2}\cos(2\epsilon) \end{pmatrix} . \tag{5.19}$$

In the present analysis, we use a simple method that directly illustrates $[\underline{S}(E)-\underline{I}]_{\alpha\beta}/2i$ $(=-\pi T_{\alpha\beta})$ by the use of an Argand diagram. This circumvents the complexity caused by the difference between the definitions of the πd and NN phase shifts.

Concerning the orthogonal set $\{\xi_i\}$ in the above discussion, as shown in Table I, the q^6 states η_i are classified in terms of the type of constituent diquark clusters and their combinations. Although the wave functions η_i are not necessarily orthogonal to each other, the original $\{\eta_i\}$, before antisymmetrization, is an orthogonal set and therefore $\{\eta_i\}$ retains the orthogonal property as a first approximation. For this reason, we use $\{\eta_i\}$ in place of $\{\xi_i\}$ to simplify the calculation in the present analysis. Taking $\{\eta_i\}$ as the basis matrix $\underline{E}^0$ becomes diagonal because the energy shift of η_i from the residual qq interaction is the sum of the Δ_{TS} of the constituent diquarks. In more exact analysis, however, one should construct an orthogonal set $\{\xi_i\}$ from $\{\eta_i\}$ by a linear transformation.

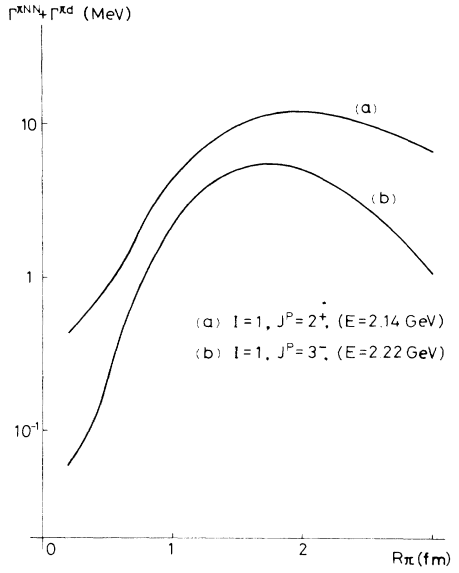

FIG. 6. $\Gamma^{\pi NN}+\Gamma^{\pi d}$ in MeV for $I=1$, $J^P=2^+$ and 3^- states as a function of R_π in fm ($\chi_2=\chi_3=1$).

VI. COMPARISON BETWEEN EXPERIMENTS AND PREDICTIONS

In the analysis of the $1p\frac{1}{2}$-shell dibaryons with $L=2$ and 3, the formulas of partial decay widths $\Gamma^{\pi NN}$, $\Gamma^{\pi d}$, and Γ^{NN}, given in Sec. IV, involve three free parameters R_π, χ_2, and χ_3. These parameters are determined by the use of experimental data for $I=1$ dibaryons. Although two states, B and C, are degenerate in $B_1^2(2.14)2^+$ as shown in Table I, it seems that the general feature of $B_1^2(2.14)2^+$ is determined solely by the state B, because if one calculates $\Gamma^{\pi NN}$, $\Gamma^{\pi d}$ and the elasticity x of the NN scattering for B and C separately, the results for C are only $\sim\frac{1}{6}$ that of B. Therefore, for the time being, we analyze $B_1^2(2.14)2^+$ simply as a single state B. A more detailed analysis is given shortly.

We show in Fig. 6 the theoretical values for $\Gamma^{\pi NN}+\Gamma^{\pi d}$ as a function of the parameter R_π where we set $\chi_2=\chi_3=1$ and the parameter R_0 is taken to be

$$R_0=0.54 \text{ fm} . \tag{6.1}$$

This is estimated from (4.8) and (4.14) with the values $m=\omega=0.300$ GeV obtained by an analysis of the dibaryon mass spectrum. As was expected, quite small values of $\Gamma^{\pi NN}+\Gamma^{\pi d}$ are obtained from small R_π values. The maximum values are obtained at around $R_\pi=1.8$ fm for both $B_1^2(2.14)2^+$ and $B_1^2(2.22)3^-$, but they are still smaller than the experimental values, which indicates that the factors χ_2 and χ_3 are considerably larger than unity. Hereafter, we continue our analysis in the region of the optimum value

$$R_\pi=1.4\text{–}2.2 \text{ fm} . \tag{6.2}$$

The parameters χ_2 and χ_3 are determined using the experimental values for $\Gamma^{\pi NN}$ of $B_1^2(2.14)2^+$ and $B_1^2(2.22)3^-$, respectively. The results are

$$\chi_2=2.4, \quad \chi_3=4.8 . \tag{6.3}$$

Here we examine the consistency of these values. Consider the generalized baryonic component Ψ^T which involves internally excited baryons. From the analysis in Sec. IV the ratio $|\Psi^B|^2/|\Psi^T|^2$ is estimated to be roughly $6^{-L}C_g{}^2$. Therefore, one obtains

$$|\chi_n\Psi^B|^2/|\Psi^T|^2\sim\begin{cases}0.27 & \text{for } B_1^2(2.14)2^+ , \\ 0.41 & \text{for } B_1^2(2.22)3^- . \end{cases} \tag{6.4}$$

These results seem to be quite reasonable, and lend support to the present analysis. We emphasize that, if one tries to fit theoretical Γ's with small R_π to experimental ones, the absolute condition $|\chi_n\Psi^B|^2\leq 1$ is severely violated. Note that the mixing probability $|\Psi^T|^2$ of the generalized baryonic component in q^6 is not small, $\sim\frac{1}{5}$ on average.

The calculated elasticity $x\,(=\Gamma^{NN}/\Gamma)$ for $B_1^2(2.14)2^+$ is 0.14 for $R_\pi=1.4$ fm and 0.05 for 1.5 fm. These values agree with the experimental value ~ 0.10. However, the theoretical x for $B_1^2(2.22)3^-$ is much smaller (only $\sim\frac{1}{5}$) than the experimental value, ~ 0.18, for $B_1^2(2.22)3^-$. This difficulty is caused by the excessively rapid decrease in the function $\zeta(h)(=e^{-R_\pi{}^2h^2/4})$ as the argument h increases. In order to solve this problem phenomenologically, we assume that the function $\zeta(h)$ involves at least two components, one of which is not sensitive to a change in h. Namely, in formulas (4.42) and (4.43), we modify the function $\zeta(h)$ using two positive parameters α and β:

$$\zeta(h)=\text{Max}[e^{-R_\pi{}^2h^2/4}, e^{-\alpha-\beta h^2}] , \tag{6.5}$$

where α and β are to be determined using the NN phase-shift data for $B_1^2(2.22)3^-$. It is true that the above modification may have some effect also on $\Gamma^{\pi NN}$, $\Gamma^{\pi d}$, and V_0,

but we neglect this in the following analysis. We note that the partial decay widths $\Gamma^{\pi NN}(E)$ and $\Gamma^{\pi d}(E)$ for $E \lesssim 2.22$ GeV (2.14 GeV), calculated by (4.26) and (4.37) are not influenced by this modification, provided that $R_\pi \lesssim 1.8$ fm (2.2 fm), and that the parameter α absorbs the variation of V_0. Therefore, the results for $E \lesssim 2.22$ GeV (2.14 GeV) are correct on the condition that $R_\pi \leq 1.8$ fm (2.2 fm). We now proceed to show the variations of the T matrix with respect to the energy E by means of Argand diagrams. Our calculation employs the formulas given in Secs. IV and V for the major low-lying dibaryons. The possible phase change δ_0 of the matrix elements caused by the initial- and final-state interactions are not taken into account in these calculations. Therefore, the comparison of the calculated Argand diagrams with the experimental ones should be done with an appropriate rotation around the center of unitarity circle.

We use the notation E_r for the theoretical resonating energy predicted by the mass formula (2.1) and, hereafter, classify the theoretical dibaryon states by I, J, and E_r as in Table I, in order to distinguish them from the dibaryon candidates $B_I^2(M)J^P$ observed experimentally. The number of the states in each group is denoted by N. The fine structure of the mass spectrum in each group is illustrated in next to the corresponding T matrix.

We begin with the analysis of $B_1^2(2.14)1^+$ because the experimental P_1 πd phase shift is available. Valuable informations can be extracted on the parameter R_π and energy shift Δ_{TS} and are shown below.

A. $I=1$, $J^P=1^+$, $E_r=2.14$ GeV, $N=4$

This level involves four states B_1, B_2, B_3, and C. The configurations of these states are given in Table I. The dibaryon candidate $B_1^2(2.14)1^+$ (Refs. 20 and 21) is assigned to this group. Adopting the one-gluon-exchange potential H_g plus the extra two-body confining potential H_c, Δ_{TS} can be written as

$$\Delta_{TS} = -\tfrac{5}{24}\Delta[1-\overline{\gamma}(-1)^{T+S}][1+2(-1)^S]+\overline{C}\ , \tag{6.6}$$

where $\overline{\gamma}$, $\overline{C}$, and Δ (>0) are the parameters which depend on H_c and H_g, respectively (Appendix D). We tried to fit the T matrix calculated by expression (6.6) to the empirical one, but this did not yield satisfactory agreement. However, a good fit is obtained by the elimination of the tensor force from H_g which eventually results in an expression

$$\Delta_{TS} = -\frac{\Delta}{4}[1-(-1)^T][1+(-1)^S]\ . \tag{6.7}$$

The parameter Δ is taken to be larger than 40 MeV. With this expression, the energy shift is given by

$$\Delta_{00}=\Delta_{01}=\Delta_{11}=0,\quad \Delta_{10}=-\Delta<-40\ \text{MeV}\ . \tag{6.8}$$

In this case, two states B_1 and B_2 keep their original resonating energy E_r ($=2.14$ GeV) while the remaining two, B_3 and C, are degenerate at the energy $E_r+\Delta_{10}$. We show in Fig. 7 the T matrix for $\Delta_{10}=-60$ MeV with $R_\pi=1.6$ and 2.0 fm by means of an Argand diagram ($-\pi\underline{T}$ is illustrated in the complex plane). As will be discussed shortly, the existing data for the narrow dibaryon

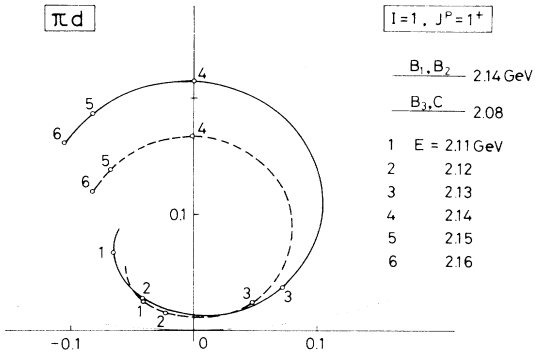

FIG. 7. The predicted πd T matrix with $I=1$, $J^P=1^+$ for $\Delta_{00}=\Delta_{01}=\Delta_{11}=0$, $\Delta_{10}=-60$ MeV, and $R_\pi=1.6$ fm (dashed curve) and 2.0 fm (solid curve) as a function of c.m. energy E. The single element $-\pi T_{11}=((S_{11}-1)/2i)$ is illustrated in the complex plane. Therefore, the radius of unitarity circle is 0.5. The fine structure of mass spectrum is illustrated on the right-hand side. The possible phase change δ_0 by initial- and final-state interactions is neglected.

resonances are well explained with this Δ_{10} value. The rapid change in the T matrix at $E\sim 2.14$ GeV is due to the small decay-strength parameters of B_2, and the reduction of the decay width of B_2 caused by the configuration mixing of B_1 and B_2. The agreement with experimental data is improved considerably by the following small correction for Δ_{01}:

$$\Delta_{00}=\Delta_{11}=0,\quad \Delta_{01}=10\ \text{MeV}\ ,$$
$$\text{and} \tag{6.9}$$
$$\Delta_{10}=-60\ \text{MeV}\ ,$$

in which B_1 and B_3 are shifted to 2.15 and 2.09 GeV, leaving B_2 and C at the original level 2.14 and 2.08 GeV, respectively. We show in Fig. 8(a) the theoretical T matrices for $R_\pi=1.8$ and 2.15 fm together with the empirical ones, where the rotation angle δ_0 in the theoretical diagram is taken to be 13°. The agreement between the two is much better at $R_\pi=2.15$ fm than at $R_\pi=1.8$ fm, but even in the poor case there is general agreement. In the following analysis, we examine both cases, $R_\pi=1.8$ and 2.15 fm, with (6.9).

The question of whether the double circles illustrated in Fig. 8(b) really exist or not will be settled only by future experiments.

B. $I=1$, $J^P=3^-$, $E_r=2.25$ GeV, $N=1$

The dibaryon candidate $B_1^2(2.22)3^-$ is assigned to this single state whose resonating energy is shifted to 2.26 GeV. The calculated NN T matrix contains two positive adjustable parameters: α and β. The optimum sets of their numerical values, i.e., the sets giving best fit to the empirical T matrix for $E<2.26$ GeV, are obtained as

$$\alpha=3.31,\quad \beta=1.00\ (\text{GeV}/c)^{-2}\ \text{for}\ R_\pi=1.8\ \text{fm}\ ,$$
$$\alpha=2.64,\quad \beta=3.68\ (\text{GeV}/c)^{-2}\ \text{for}\ R_\pi=2.15\ \text{fm}\ . \tag{6.10}$$

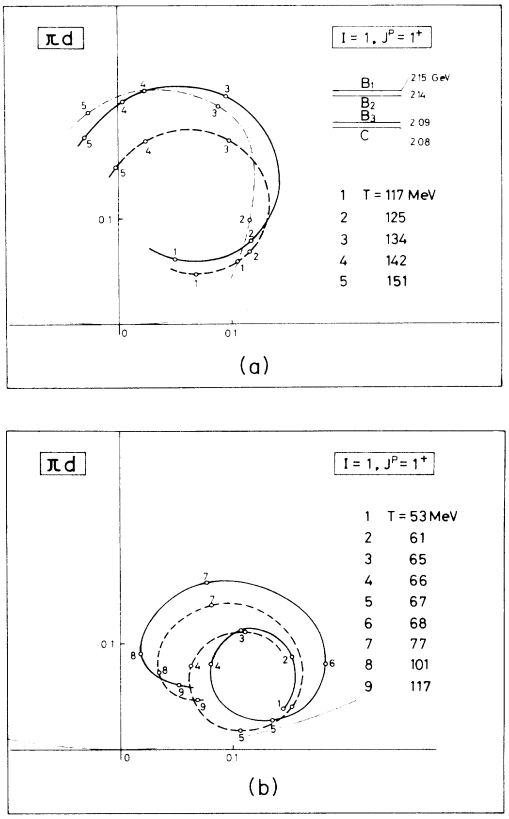

FIG. 8. Comparison of theoretical and experimental πd T matrices with $I=1$, $J^P=1^+$ by means of an Argand diagram. The dashed and solid curves are the predictions for $R_\pi=1.8$ and 2.15 fm, respectively, with energy shift (6.9), while the dashed-dotted curve is from phase-shift analysis by Ref. 21. The theoretical diagrams are rotated by δ_0 ($=13°$) around the center of unitarity circle. (a) The result for $T \geq 117$ MeV (T: pion laboratory energy). (b) The result for $T \leq 117$ MeV. There is no phase-shift analysis for $T < 117$ MeV.

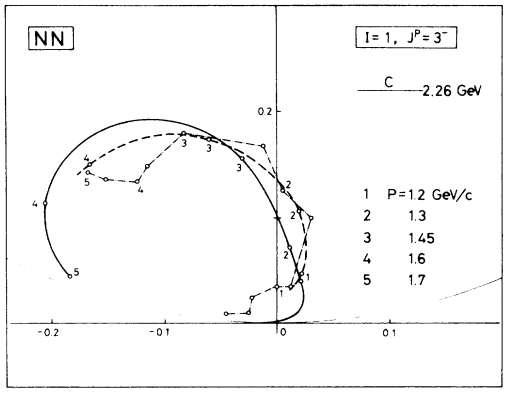

FIG. 9. The Argand diagram for the NN T matrix with $I=1$, $J^P=3^-$ as a function of laboratory momentum P. The dashed and solid curves are the results for $R_\pi=1.8$ fm, $\chi_3=4.8$, and $R_\pi=2.15$ fm, $\chi_3=4.0$, respectively, with parameter (6.9) and $\delta_0=-18°$. The dashed-dotted curve stands for the phase-shift analysis by Hoshizaki (Ref. 14).

The Argand diagrams of the calculated T matrix are illustrated in Figs. 9 and 10 where a slightly smaller parameter $\chi_3=4.0$ is taken for $R_\pi=2.15$ fm. In the comparison with the empirical NN T matrix ($\delta_0=-18°$), the result for $R_\pi=1.8$ fm seems better than for $R_\pi=2.15$ fm case. But a definite conclusion may not be obtained because the results for $R_\pi=2.15$ fm should be corrected in this energy range for the modification given in (6.5). As shown in Table II, the decay-strength parameters with $l \neq L$ vanish in this state. Therefore, the ratio ϵ ($=T_{12}/T_{11}$) for the πd T matrix defined by Kubodera *et al.*,[38] is determined only by the decay-strength parameters and kinematical constants $A^{NB}(l_k l_q l_t S_k : lS)$. It is expected to be

$$\epsilon = \frac{\sqrt{3}}{2} . \tag{6.11}$$

It should be noted that this constant reflects the q^6 structure in the diquark-cluster model and is independent of the decay dynamics.

C. $I=1$, $J^P=2^+$, $E_r=2.14$ GeV, $N=2$

Candidate $B_1^2(2.14)2^+$ is assigned to this level in which state B is shifted to 2.15 GeV. The T matrices are given in Figs. 11 and 12. The small structure observed at 2.14 GeV in the NN T matrix ($\delta_0=15°$) and the P-wave, πd T matrix is caused by C. This C-induced small structure becomes a prominent circle with $\Gamma \sim 4$ MeV in the F-wave πd T matrix through the interference with B. At this point, this structure is not small and careful analysis is required for ther πd phase-shift analysis at 2.14 GeV.

As was expected, the influence of C on the general features of the T matrix is not important except for the F-wave, πd channel.

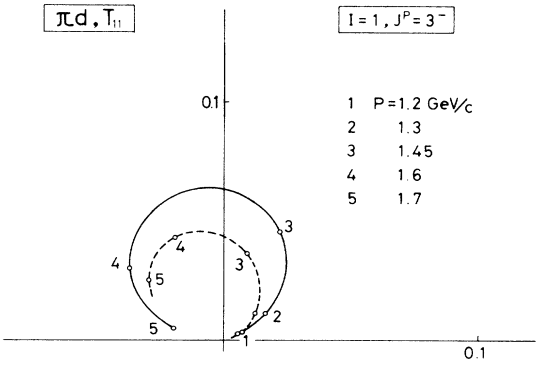

FIG. 10. The predictions for $-\pi T_{11}$ with $I=1$, $J^P=3^-$ ($\delta_0=0°$), where the matrix

$$\begin{bmatrix} T_{11} & T_{12} \\ T_{21} & T_{22} \end{bmatrix}$$

represents the πd T matrix. The subscripts 1 and 2 represent $l_q=J-1$ and $J+1$ states, respectively. The other elements $T_{12}(=T_{21})$ and T_{22} are given by formulas $T_{12}=(\sqrt{3}/2)T_{11}$ and $T_{22}=\frac{3}{4}T_{11}$.

TABLE II. The decay-strength parameter $\epsilon_D^{BB'}(LlS)$ and factor D_N. Unnecessary elements are not listed.

I	J^P		D_N	$\epsilon_D^{NN}(331)$	$\epsilon_D^{N\Delta}(331)$	$\epsilon_D^{N\Delta}(332)$	$\epsilon_D^{N\Delta}(312)$	
1	3^-	C	$(\frac{2}{3})^{1/2}$	$\frac{4}{27}\sqrt{10}$	$-\frac{16}{27}(\frac{1}{5})^{1/2}$	0	0	
				$\epsilon_D^{NN}(220)$	$\epsilon_D^{N\Delta}(221)$	$\epsilon_D^{N\Delta}(222)$	$\epsilon_D^{N\Delta}(202)$	$\epsilon_D^{\Delta\Delta}(202)$
1	2^+	B	1	$\frac{4}{3}(\frac{1}{15})^{1/2}$	$\frac{2}{3}(\frac{1}{5})^{1/2}$	$-\frac{2}{3}(\frac{7}{15})^{1/2}$	$-\frac{2}{3}(\frac{1}{15})^{1/2}$	0
		C	1	$\frac{2}{9}(\frac{1}{15})^{1/2}$	$\frac{2}{3}(\frac{1}{5})^{1/2}$	$-\frac{2}{9}(\frac{7}{15})^{1/2}$	$-\frac{2}{9}(\frac{1}{15})^{1/2}$	$-\frac{2}{9}(\frac{2}{3})^{1/2}$
				$\epsilon_D^{N\Delta}(221)$	$\epsilon_D^{N\Delta}(222)$	$\epsilon_D^{N\Delta}(201)$		
1	1^+	B_1	1	$-\frac{4}{9}$	0	$-\frac{2}{9}(\frac{1}{5})^{1/2}$		
		B_2	1	$-\frac{1}{9}\sqrt{2}$	$-\frac{1}{3}\sqrt{2}$	$-\frac{2}{9}(\frac{2}{5})^{1/2}$		
		B_3	1	$\frac{1}{3}\sqrt{2}$	$-\frac{1}{3}\sqrt{2}$	0		
		C	1	$\frac{2}{9}$	$-\frac{2}{9}$	$-\frac{2}{9}(\frac{1}{5})^{1/2}$		
				$\epsilon_D^{N\Delta}(222)$	$\epsilon_D^{NN}(200)$	$\epsilon_D^{\Delta\Delta}(200)$		
1	0^+	B_1	$(\frac{8}{11})^{1/2}$	$\frac{2}{3}(\frac{1}{3})^{1/2}$	$-\frac{2}{3}(\frac{5}{3})^{1/2}$	0		
		B_2	$\frac{2}{3}\sqrt{2}$	$-\frac{2}{3}$	$-\frac{2}{3}(\frac{1}{5})^{1/2}$	0		
		C_1	$\frac{2}{3}\sqrt{2}$	$\frac{2}{9}(\frac{1}{3})^{1/2}$	$\frac{4}{9}(\frac{1}{15})^{1/2}$	$\frac{8}{9}(\frac{1}{3})^{1/2}$		
		C_2	$\frac{2}{3}\sqrt{2}$	$-\frac{2}{9}$	$-\frac{2}{9}(\frac{1}{5})^{1/2}$	$\frac{4}{9}$		
				$\epsilon_D^{NN}(330)$				
0	3^-	D	$(\frac{2}{3})^{1/2}$	$\frac{2}{3}(\frac{2}{15})^{1/2}$				
				$\epsilon_D^{NN}(221)$	$\epsilon_D^{NN}(201)$	$\epsilon_D^{\Delta\Delta}(201)$		
0	1^+	A_1	$\frac{2}{3}\sqrt{2}$	$\frac{2}{3}$	$\frac{4}{3}(\frac{1}{5})^{1/2}$	0		
		A_2	$\frac{2}{3}\sqrt{2}$	$\frac{2}{3}$	$-\frac{2}{3}(\frac{1}{5})^{1/2}$	0		
		C_1	$(\frac{8}{11})^{1/2}$	$\frac{4}{9}(\frac{1}{3})^{1/2}$	$\frac{14}{9}(\frac{1}{15})^{1/2}$	$\frac{4}{9}(\frac{1}{3})^{1/2}$		
		C_2	$(\frac{8}{11})^{1/2}$	$\frac{4}{9}(\frac{1}{3})^{1/2}$	$-\frac{2}{9}(\frac{5}{3})^{1/2}$	$-\frac{8}{9}(\frac{1}{3})^{1/2}$		

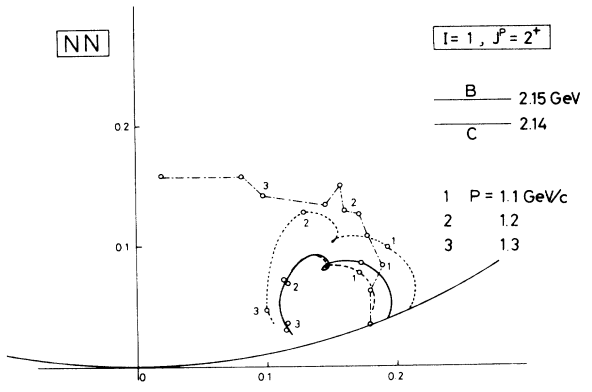

FIG. 11. The Argand diagram for the NN T matrix with $I=1$, $J^P=2^+$ as a function of P. Dashed and solid curves are the results for $R_\pi=1.8$ and 2.15 fm, respectively, with the resonating energy $E_r=2.14$ GeV and the parameter $\chi_2=2.4$, energy shift (6.9), and $\delta_0=15°$. The dotted curve is the result for $R_\pi=2.15$ fm and $E_r=2.15$ GeV calculated dropping the exchange term. The dashed-dotted curve stands for the phase-shift analysis by Hoshizaki (Ref. 14).

At first sight it seems as if there existed non-negligible discrepancy between theoretical and experimental NN T matrices. Actual discrepancy, however, may be smaller, because we have to take into account the effect of the nonresonant absorption caused by S-wave $N\Delta$ intermediate state, which may show rapid increase around the $N\Delta$ threshold, 2.17 GeV. Incidentally, restricting ourselves on this part of the NN T matrix, a clear agreement between theory and experiment would be obtained, if we assumed a slightly higher resonating energy, $E_r=2.15$ GeV, and, at the same time, omitted the exchange term $m_N^{\rm ex}(l_k)$ in (4.47). It is shown in Fig. 11. We, however, cannot adopt this choice, because of the following two reasons. First, this modification in E_r affects the T matrix with $I=1$, $J^P=1^+$ in an undesirable manner. Second, the omission of the exchange term makes the clear resonance at 2.14 GeV disappear in the calculated NN T matrix with $I=1$, $J^P=0^+$, and thus makes impracticable the analysis in the next paragraph, in which we assign one of the four states with $I=1$, $J^P=0^+$ to a narrow resonance observed at 2.14 GeV by the Rice-LAMPF group.[39]

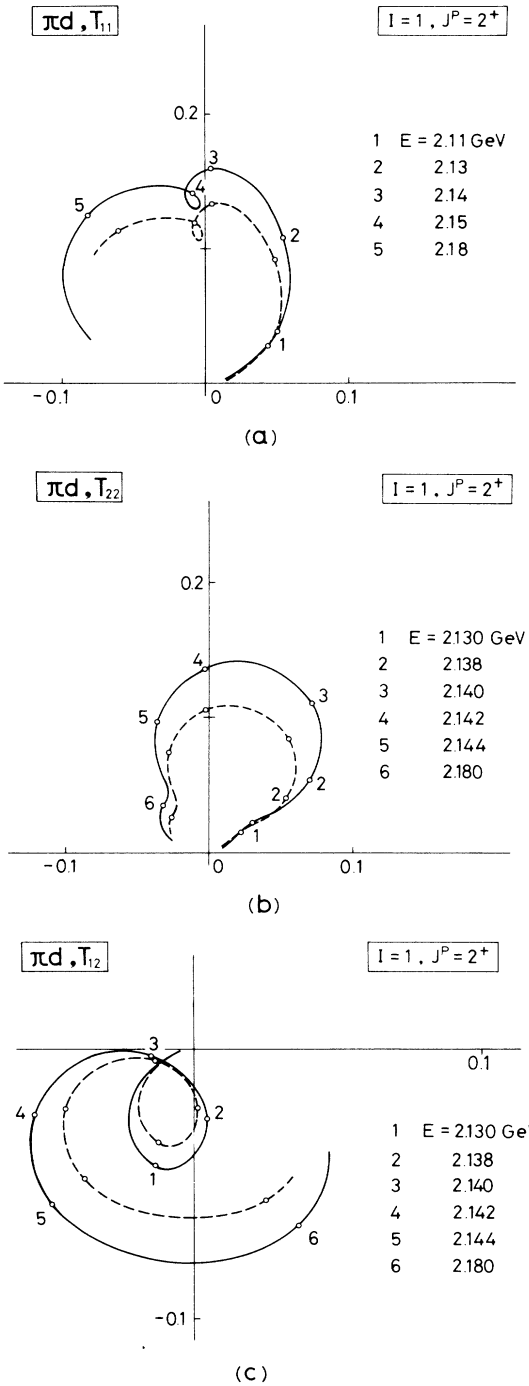

FIG. 12. Predictions for the πd T matrix with $I=1$, $J^P=2^+$ ($\delta_0=0°$) as a function of c.m. energy E. Case (a) shows $-\pi T_{11}$, (b) $-\pi T_{22}$, and (c) $-\pi T_{12}$ ($=-\pi T_{21}$).

D. $I=1$, $J^P=0^+$, $E_r=2.14$ GeV, $N=4$

Four states B_1, B_2, C_1, and C_2 are involved in this level. One state C_1 stays at $E=2.14$ GeV while B_1, B_2, and C_2 are shifted to 2.15, 2.08, and 2.02 GeV, respectively. The predicted Argand diagram for the NN T matrices are

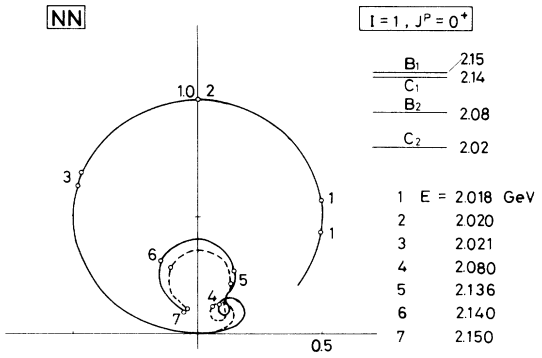

FIG. 13. Predictions for the NN T matrix with $I=1$, $J^P=0^+$ ($\delta_0=0°$) as a function of E. The same parameters R_π, χ_2, and Δ_{TS} as Fig. 11 are used.

shown in Fig. 13, where two clear defined circles are found at 2.02 and 2.14 GeV and a structure at 2.08 GeV is observed. The narrow resonance (circle) with $x\sim0.4$ and $\Gamma\sim10$ MeV, at 2.14 GeV, is due to C_1. This resonance may be consistent with a sharp peak at 2.14 GeV which was found by the Rice-LAMPF group[39] in their experimental analysis of the $\Delta\sigma_T$ in pp scattering. In fact, this peak can be interpreted as a $^1S_0$ pp resonance with $x\sim0.4$ and $\Gamma\sim20$ MeV and is consistent with our result as shown in Fig. 13. Further support for the existence of this narrow resonance at 2.14 GeV comes from the invariant mass experiments of the $dp\rightarrow(np)p$ breakup reactions by Siemiarzuk *et al.*,[25] in which they found narrow, two nucleon enhanced peaks at 2.13 and 2.02 GeV. Of course, the partner at 2.02 GeV can be assigned to the large (narrow) resonance C_2 at 2.02 GeV as shown in Fig. 13. The effect of B_2 on the NN T matrix is small and observed as a structure at 2.08 GeV.

Concerning the T matrix of the πd channel (Fig. 14), a prominent B_2 resonance with $\Gamma\sim30$ MeV is observed at 2.08 GeV. A relatively large elasticity $x_d=0.2$–0.3 indicates a strong coupling of B_2 to the πd channel, and the

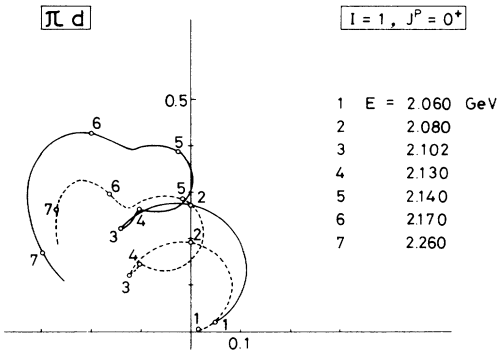

FIG. 14. Predictions for the πd T matrix with $I=1$, $J^P=0^+$ ($\delta_0=0°$). The same parameters R_π, χ_2, and Δ_{TS} as Fig. 11 are used.

mixing probability of the B_2 n component in ^{3}He may not be small. Therefore, dibaryons B_2 should be produced in large numbers in the reaction

$$^3\text{He}+p\rightarrow d+B_2$$

via a neutron pickup from the B_2 n component. The narrow peak at 2.12 GeV with $\Gamma\sim 50$ MeV, observed in the missing-mass experiment[24] ($^3\text{He}+p\rightarrow d+$ anything) can be interpreted as the production of B_2. We remark that the observation of B_2 by NN invariant-mass experiments may be difficult as B_2 has a small x value (~ 0.05).

E. $I=0$, $J^P=3^-$, $E_r=2.25$ GeV, $N=1$

Candidate $B_0^2(2.22)3^-$ is assigned to this level, which is composed of a single state, as its partner $B_1^2(2.22)3^-$. The T matrix is given in Fig. 15. Our theory predicts the following values for the partial decay widths:

$$\Gamma=40.8 \text{ MeV and } \Gamma^{NN}=7.7 \text{ MeV for } R_\pi=1.8 \text{ fm},$$
$$\Gamma=20.5 \text{ MeV and } \Gamma^{NN}=4.0 \text{ MeV for } R_\pi=2.15 \text{ fm}. \tag{6.12}$$

These values are consistent with Hoshizaki's results[23]

$$\Gamma\sim 50 \text{ MeV and } \Gamma^{NN}\sim 6 \text{ MeV},$$

obtained by a phase-shift analysis. It is easily seen from (4.42) and (4.53) that the ratio of the Γ^{NN}s for $B_0^2(2.22)3^-$ and $B_1^2(2.22)3^-$ equals the square of the ratio of the corresponding decay-strength parameters. Namely, the present model predicts

$$\Gamma^{NN}(B_0^2(2.22)3^-)/\Gamma^{NN}(B_1^2(2.22)3^-)=\tfrac{27}{100}. \tag{6.13}$$

Note that this ratio reflects the q^6 structure of the diquark-cluster model as the parameter ϵ given in (6.11).

F. $I=0$, $J^P=1^+$, $E_r=2.14$ GeV, $N=4$

This level involves four states A_1, A_2, C_1, and C_2. The resonating energy of A_1, A_2, and C_2 are shifted to 2.16, 2.15, and 2.08 GeV, respectively, while C_1 stays at 2.14 GeV. The T matrix is illustrated in Fig. 16. The large resonance at 2.08 GeV with $\Gamma\sim 20$ MeV is caused by C_2. The relatively small resonance at 2.14 GeV with $\Gamma\sim 10$ MeV is dominated by C_1. We emphasize that these two resonances have sufficiently large elasticity and moderate Γ value and, therefore, they should be observ-

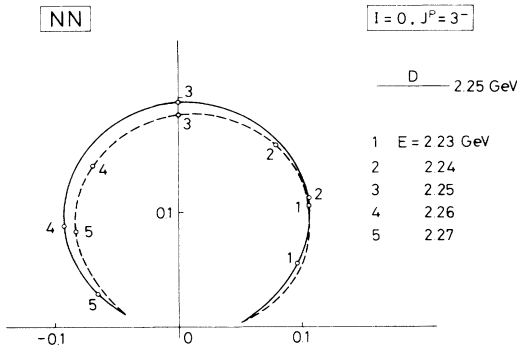

FIG. 15. Predictions for the NN T matrix with $I=0$, $J^P=3^-$ ($\delta_0=0°$). The same parameters R_π, χ_3, and Δ_{TS} as Fig. 9 are used.

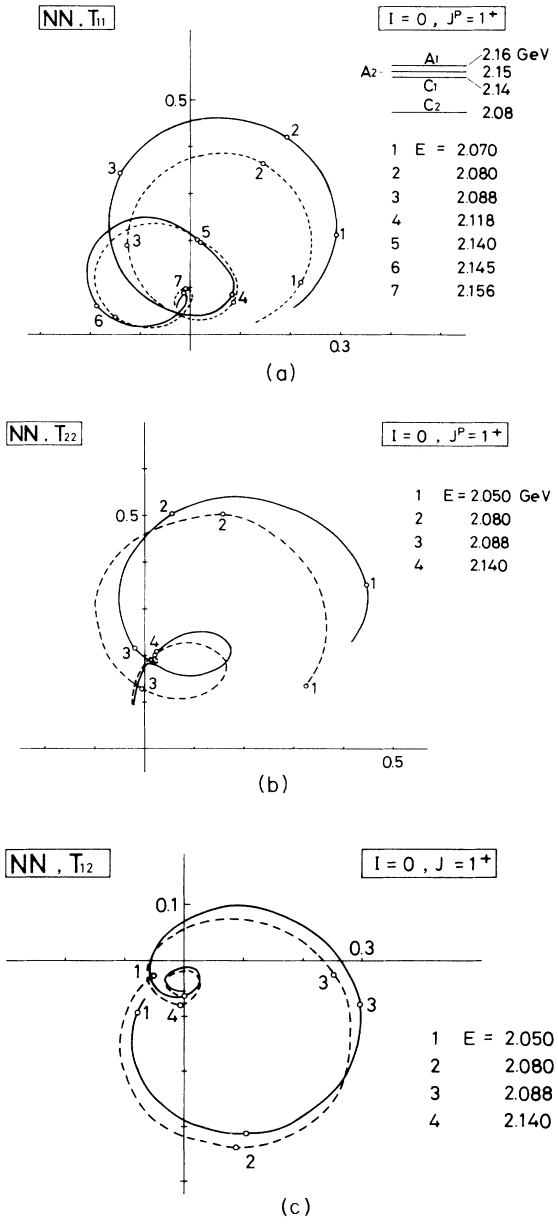

FIG. 16. Predictions for the NN T matrix

$$\begin{pmatrix} T_{11} & T_{12} \\ T_{21} & T_{22} \end{pmatrix}$$

with $I=0$, $J^P=1^+$ ($\delta_0=0°$). The subscripts 1 and 2 represent $l_k=J-1$ and $J+1$ states, respectively. Case (a) shows $-\pi T_{11}$, (b) $-\pi T_{22}$, and (c) $-\pi T_{12}$ ($=-\pi T_{21}$). The same parameters R_π, χ_2, and Δ_{TS} as Fig. 11 are used.

able in the experiments of np scattering which has started in LAMPF.

As shown in Fig. 2, several observable $1p\frac{1}{2}$-shell dibaryons remain in the energy region 2.10—2.30 GeV. These dibaryons involve many states (≥ 10) with the same quantum numbers in a narrow energy range and extremely careful and sophisticated analysis is required. Our analysis will appear elsewhere.

Three groups of q^6 states with $I=1$ and $J^P=2^-$, $1^-,0^-$ having configurations $[(1s\frac{1}{2})^2]^2[(1p\frac{1}{2})(1s\frac{1}{2})]$, $[(1p\frac{1}{2})(1s\frac{1}{2})]^3$, and $[(1s\frac{1}{2})^2][(1p\frac{1}{2})(1s\frac{1}{2})][(1p\frac{1}{2})^2]$, are distributed over a range 2.19—2.29 GeV for $J^P=2^-$, and 2.13—2.29 GeV for $J^P=1^-$ and 0^-. The πd and NN T matrices influenced by these q^6 states likely have a very complicated structure. In fact, all of the experimental phase shifts for the $J^P=2^-,1^-,0^-$ channels exhibit complex structures.[40] The existence of two dibaryon candidates with $J^P=2^-$ at ~ 2.19 GeV suggested by Yokosawa[2,3] and the one at 2.32 GeV suggested by Hoshizaki[40] may reflect this situation. The diquark-cluster model predicts that similar complex structure will be observed in the T matrix of $^1P_1$ NN scattering, because this channel is under the strong influence of a group of q^6 states with $I=0$ and $J^P=1^-$ distributed in the range 2.13—2.29 GeV.

When many states with the same quantum numbers exist in a narrow energy region as in the above cases, under some circumstances, a clear resonating state with a narrow decay width can be produced by the mixing of different configurations. The narrow dibaryon candidates at 2.19 GeV with $\Gamma\sim 50$ MeV and at 2.24 GeV with $\Gamma\sim 32$ MeV, observed in missing-mass experiments with light nuclei,[24] can be interpreted as one of these special resonating states.

We point out that, in a family of $1d\frac{3}{2}$-shell dibaryons with $I=0$ and $J^P=4^+,3^+,\ldots,0^+$, $E_r=2.475$ GeV, and the configuration $[(1p\frac{1}{2})(1s\frac{1}{2})]^2[(1d\frac{3}{2})(1s\frac{1}{2})]$, the members with $J^P=3^+$ involving a [10] diquark can be interpreted as $B_0^2(2.38)3^+$ because their rest mass is shifted by Δ_{10} (~ -60 MeV) and it becomes close to ~ 2.38 GeV.

In conclusion we note that the diquark-cluster model seems to be successful in reproducing the general features of the dibaryon spectrum involving the partial decay widths.

VII. CONCLUDING REMARKS

Utilizing a semiphenomenological approach for modeling the decay dynamics of dibaryons, we were able to generate predictions for the πd and NN T matrices.

With the diquark-cluster model, we have succeeded in reproducing the experimental T matrix for a narrow dibaryon $B_1^2(2.14)1^+$ coexisting with a broad $B_1^2(2.14)2^+$. The calculated partial decay widths for $B_0^2(2.22)3^-$ are quite consistent with Hoshizaki's results. We remark that the diquark-cluster model can predict the existence of the narrow dibaryon resonances at 2.02 and 2.13 GeV found by Siemiarzuk *et al.*, and the one at 2.12 GeV found by Tatischeff *et al.*, as well as the one at 2.14 GeV suggested by the Rice-LAMPF group. In future experiments, confirmation of the existence of the narrow dibaryons with $I=0$ and $J^P=1^+$ at 2.08 and 2.14 GeV should be the ical goal of diquark-cluster model analysis. Further precise experimental analysis of the $P_1\pi d$ phase shift at around 2.08 GeV and the $^1S_0$ pp phase shift at 2.02 and 2.14 GeV may provide other tests for the diquark-cluster model. We have found phenomenologically that, by the elimination of the tensor force from the one-gluon-exchange qq interaction, a favorable expression for the energy shift Δ_{TS} in the P-wave diquark is obtained. The reason why the tensor force vanishes in the P-wave diquark is a theoretically open question. Concerning further analysis, in Sec. II we concluded that the major high-lying q^6 states (above 2.3 GeV) are a series of $1d\frac{3}{2}$-shell dibaryons. Our task is, of course, to calculate the partial widths of these $1d\frac{3}{2}$-shell dibaryons as well as the remaining minor $p\frac{1}{2}$-shell dibaryons. An important difference between the reactions with energy below and above 2.3 GeV may be the relative weight of any two-pion-production processes. In the present analysis, we assumed that the transformation of the q^6 system proceeds via a one-pion emission from a baryon cluster until the fission of the system occurs. But what will happen with a two-pion emission from baryon clusters? If the spectator baryon cluster B_c' in Fig. 3 emits the second pion, it may also take part in the system transformation. This implies that the two-pion-production processes of a q^6 system are not simple replications of the one-pion-production processes and a more sophisticated analysis is required. We will discuss this problem in a forthcoming paper.

ACKNOWLEDGMENTS

We are grateful to Dr. A. Yokosawa (Argonne National Laboratory) for his helpful advice. A special acknowledgment is due to Dr. D. Green (Hosei University) for careful reading of the manuscript. We also wish to thank the Computer Center of Hosei University at Tama for the use of FACOM-M360R computer.

APPENDIX A: DECAY-STRENGTH PARAMETER $\epsilon^{BB'}(LlS)$

In order to calculate the $\epsilon^{BB'}(nlS)$ in (4.19), one must look more closely at the expression of $Z^{BB'}(lS)$ given in (4.21). The wave function Φ^{JJ} can be written as

$$\Phi^{JJ}=\Phi_c(12,34,56)\Phi_t(l_1l_2\cdots l_6)\ , \tag{A1}$$

where $\Phi_c(12,34,56)$ and $\Phi_t(l_1l_2\cdots l_6)$ are normalized color and isospin-spin angular wave functions, respectively, of the q^6 system as illustrated in Fig. 1. The subsets (q_1q_2), (q_3q_4), and (q_5q_6) form three diquarks d_1, d_2, and d_3, respectively. Because the $\Phi_c(12,34,56)$ is antisymmetrical with respect to the exchange of the two quarks involved in a diquark, as well as for the interchange of the two diquarks, formula (4.7) can be written as

$$\Psi=N_m\sum{}'(-)\Phi_c(12,34,56)\Phi_t(12,34,56)\ , \tag{A2}$$

$$N_m=N_a/N_r\ . \tag{A3}$$

where

TABLE III. Coefficients $A^{NB}(l_k l_q l_t S_k : lS)$. Unnecessary elements are not listed.

(a) $I=1$ and $J^P=3^-$

$A^{NN}(l_k l_q l_t S_k:31)$		$A^{N\Delta}(l_k l_q l_t S_k:31)$		$A^{N\Delta}(l_k l_q l_t S_k:32)$		$A^{N\Delta}(l_k l_q l_t S_k:12)$	
(0221:31)	$\frac{2}{\sqrt{21}}$	(0221:31)	$-\frac{2}{\sqrt{21}}$	(0221:32)	$2(\frac{3}{35})^{1/2}$	(0221:12)	$-\frac{2}{\sqrt{5}}$
(0441:31)	$\frac{1}{\sqrt{7}}$	(0441:31)	$-\frac{1}{\sqrt{7}}$	(0441:32)	$-\frac{1}{3}(\frac{5}{7})^{1/2}$		
(1121:31)	$\frac{4}{3}(\frac{7}{5})^{1/2}$	(1121:31)	$\frac{2}{3}(\frac{7}{5})^{1/2}$	(1121:32)	$-\frac{2}{5}\sqrt{7}$	(1121:12)	$(\frac{1}{3})^{1/2}$
(1321:31)	$-\frac{2}{3}(\frac{2}{105})^{1/2}$	(1321:31)	$-\frac{1}{3}(\frac{2}{105})^{1/2}$	(1321:32)	$\frac{1}{5}(\frac{2}{21})^{1/2}$		
(1331:31)	$\frac{1}{6}(\frac{2}{3})^{1/2}$	(1331:31)	$\frac{1}{6}(\frac{1}{6})^{1/2}$	(1331:32)	$\frac{1}{2}(\frac{5}{6})^{1/2}$		
(1341:31)	$3(\frac{3}{14})^{1/2}$	(1341:31)	$\frac{3}{2}(\frac{3}{14})^{1/2}$	(1341:32)	$\frac{1}{2}(\frac{15}{14})^{1/2}$		
(2021:31)	$\frac{2}{3}(\frac{7}{3})^{1/2}$	(2021:31)	$-\frac{2}{3}(\frac{7}{3})^{1/2}$	(2021:32)	$2(\frac{7}{15})^{1/2}$		
(2221:31)	$-\frac{2}{3}(\frac{2}{15})^{1/2}$	(2221:31)	$\frac{2}{3}(\frac{2}{15})^{1/2}$	(2221:32)	$-\frac{2}{5}(\frac{2}{3})^{1/2}$		
(2231:31)	$\frac{1}{6}(\frac{14}{15})^{1/2}$	(2231:31)	$-\frac{1}{6}(\frac{14}{15})^{1/2}$	(2231:32)	$-(\frac{7}{6})^{1/2}$		
(2241:31)	$\frac{3}{2}(\frac{2}{5})^{1/2}$	(2241:31)	$-\frac{3}{2}(\frac{2}{5})^{1/2}$	(2241:32)	$-(\frac{1}{2})^{1/2}$		
(3121:31)	$-\frac{2}{3}(\frac{10}{21})^{1/2}$	(3121:31)	$-\frac{1}{3}(\frac{10}{21})^{1/2}$	(3121:32)	$(\frac{2}{21})^{1/2}$		
(3131:31)	$\frac{1}{6}(\frac{2}{3})^{1/2}$	(3131:31)	$\frac{1}{6}(\frac{1}{6})^{1/2}$	(3131:32)	$\frac{1}{2}(\frac{5}{6})^{1/2}$		
(3141:31)	$(\frac{3}{14})^{1/2}$	(3141:31)	$\frac{1}{2}(\frac{3}{14})^{1/2}$	(3141:32)	$\frac{1}{4}(\frac{10}{21})^{1/2}$		
(1330:31)	$\frac{1}{3}$	(1330:31)	$\frac{2}{3}$	(1330:32)	0		
(2230:31)	$\frac{2}{3}(\frac{7}{5})^{1/2}$	(2230:31)	$-\frac{2}{3}(\frac{7}{5})^{1/2}$	(2230:32)	0		
(3130:31)	$\frac{1}{3}$	(3130:31)	$\frac{2}{3}$	(3130:32)	0		

(b) $I=1$ and $J^P=2^+$

$A^{NN}(l_k l_q l_t S_k:20)$		$A^{N\Delta}(l_k l_q l_t S_k:21)$		$A^{N\Delta}(l_k l_q l_t S_k:22)$		$A^{N\Delta}(l_k l_q l_t S_k:02)$	
(0111:20)	$(\frac{2}{15})^{1/2}$	(0111:21)	$(\frac{1}{5})^{1/2}$	(0111:22)	$-(\frac{7}{15})^{1/2}$	(0111:02)	$(\frac{2}{3})^{1/2}$
(0331:20)	$-(\frac{1}{5})^{1/2}$	(0331:21)	$(\frac{2}{15})^{1/2}$	(0331:22)	$(\frac{2}{35})^{1/2}$		
(1011:20)	$\frac{2}{3}(\frac{5}{3})^{1/2}$	(1011:21)	$-\frac{1}{3}(\frac{5}{2})^{1/2}$	(1011:22)	$\frac{1}{3}(\frac{35}{6})^{1/2}$		
(1211:20)	$-\frac{1}{3}(\frac{2}{15})^{1/2}$	(1211:21)	$\frac{1}{6}(\frac{1}{5})^{1/2}$	(1211:22)	$-\frac{1}{6}(\frac{7}{15})^{1/2}$		
(1221:20)	$\frac{\sqrt{2}}{3}$	(1221:21)	$-\frac{1}{6}(\frac{1}{3})^{1/2}$	(1221:22)	$-\frac{1}{6}\sqrt{7}$		
(1231:20)	$-\frac{2}{3}(\frac{14}{5})^{1/2}$	(1231:21)	$-\frac{2}{3}(\frac{7}{15})^{1/2}$	(1231:22)	$-\frac{2}{3}(\frac{1}{5})^{1/2}$		
(2111:20)	$-(\frac{1}{15})^{1/2}$	(2111:21)	$-(\frac{1}{10})^{1/2}$	(2111:22)	$\frac{1}{2}(\frac{14}{15})^{1/2}$		
(2121:20)	$\frac{1}{3}$	(2121:21)	$\frac{1}{6}(\frac{2}{3})^{1/2}$	(2121:22)	$\frac{1}{6}\sqrt{14}$		
(2131:20)	$-\frac{1}{3}(\frac{7}{5})^{1/2}$	(2131:21)	$\frac{1}{3}(\frac{14}{15})^{1/2}$	(2131:22)	$\frac{1}{3}(\frac{2}{5})^{1/2}$		
		(1220:21)	$-\frac{2}{3}$				
		(2120:21)	$\frac{\sqrt{2}}{3}$				

(c) $I=1$ and $J^P=1^+$

$A^{N\Delta}(l_k l_q l_t S_k:21)$		$A^{N\Delta}(l_k l_q l_t S_k:22)$		$A^{N\Delta}(l_k l_q l_t S_k:01)$	
(0111:21)	$\frac{1}{3}$	(0111:22)	-1	(0111:01)	$\frac{\sqrt{2}}{3}$
(1011:21)	$-\frac{5}{9}(\frac{1}{2})^{1/2}$	(1011:22)	$\frac{5}{3}(\frac{1}{2})^{1/2}$		
(1211:21)	$\frac{1}{18}$	(1211:22)	$-\frac{1}{6}$		
(1221:21)	$-\frac{1}{2}(\frac{1}{3})^{1/2}$	(1221:22)	$-\frac{1}{2}(\frac{1}{3})^{1/2}$		
(2111:21)	$-\frac{1}{3}(\frac{1}{2})^{1/2}$	(2111:22)	$(\frac{1}{2})^{1/2}$		
(2121:21)	$\frac{1}{2}(\frac{2}{3})^{1/2}$	(2121:22)	$(\frac{1}{6})^{1/2}$		

TABLE III. (*Continued*).

(c) $I=1$ and $J^P=1^+$

$A^{N\Delta}(l_k l_q l_t S_k{:}21)$		$A^{N\Delta}(l_k l_q l_t S_k{:}22)$		$A^{N\Delta}(l_k l_q l_t S_k{:}01)$	
(0110:21)	$-\frac{2}{3}$			(0110:01)	$\frac{\sqrt{2}}{3}$
(1010:21)	$\frac{10}{9}\sqrt{2}$				
(1210:21)	$-\frac{2}{9}$				
(2110:21)	$\frac{\sqrt{2}}{3}$				

(d) $I=1$ and $J^P=0^+$

$A^{NN}(l_k l_q l_t S_k{:}00)$		$A^{N\Delta}(l_k l_q l_t S_k{:}22)$	
(0111:00)	$-(\frac{1}{3})^{1/2}$	(0111:22)	$-\frac{2}{\sqrt{3}}$
		(1011:22)	$\frac{5}{3}(\frac{2}{3})^{1/2}$
		(1211:22)	$-\frac{1}{3}(\frac{1}{3})^{1/2}$
		(2111:22)	$(\frac{2}{3})^{1/2}$

(e) $I=0$ and $J^P=3^-$

$A^{NN}(l_k l_q l_t S_k{:}30)$		$A^{NN}(l_k l_q l_t S_k{:}30)$	
(1121:30)	$-(\frac{14}{5})^{1/2}$	(3121:30)	$(\frac{5}{21})^{1/2}$
(1321:30)	$(\frac{1}{105})^{1/2}$	(3131:30)	$-(\frac{1}{3})^{1/2}$
(1331:30)	$-(\frac{1}{3})^{1/2}$	(3141:30)	$(\frac{3}{7})^{1/2}$
(1341:30)	$3(\frac{3}{7})^{1/2}$		

(f) $I=0$ and $J^P=1^+$

$A^{NN}(l_k l_q l_t S_k{:}21)$		$A^{NN}(l_k l_q l_t S_k{:}21)$		$A^{NN}(l_k l_q l_t S_k{:}01)$	
(0110:21)	$(\frac{2}{3})^{1/2}$	(1011:21)	$-\frac{5}{3}(\frac{1}{3})^{1/2}$	(0110:01)	$-(\frac{1}{3})^{1/2}$
(2110:21)	$-(\frac{1}{3})^{1/2}$	(1211:21)	$\frac{1}{3}(\frac{1}{6})^{1/2}$		
		(1221:21)	$-(\frac{1}{2})^{1/2}$		

$$\Phi_t(12,34,56)=N_t N_s \sum{}''(-)''\Phi_t(l_1 l_2\cdots l_6) r_1^{l_1} r_2^{l_2}\cdots r_6^{l_6} e^{-(r_1^2+r_2^2+\cdots+r_6^2)/2R^2} . \tag{A4}$$

The summation $\sum'$ runs over all possible permutations which produce different partitions of six quarks into three diquarks. The summation $\sum''$ runs over the possible interchange of diquarks d_1, d_2, and d_3, and also the exchange of two quarks involved in a diquark. The factor $(-)''$ is $+1$ for even permutations of d_1, d_2, and d_3 and -1 for odd ones, being independent of the exchange of two quarks in a diquark. The normalization constant N_t is determined by a condition

$$\int |\Phi_t(12,34,56)|^2 d^3r_1 d^3r_2\cdots d^3r_6=1 . \tag{A5}$$

On the other hand, the wave function $\Phi^{BB'}(IlSJ{:}\mathbf{r})$ can be also written as

$$\Phi^{BB'}(IlSJ{:}\mathbf{r})=\Phi_c^{BB'}(123,456)\Phi_t^{BB'}(IlSJ{:}\mathbf{r}) , \tag{A6}$$

where $\Phi_c^{BB'}(123,456)$ and $\Phi_t^{BB'}(IlSJ{:}\mathbf{r})$ represents normalized color and isospin-spin-angular wave functions, respectively. Calculating (4.21), with use of expressions (A2) and (A6), among 15 terms for the summation $\sum'$, nine of those produce an identical result and the remaining six terms vanish. By a simple calculation, one obtains

$$\langle \Phi_c^{BB'}(123,456)\,|\,\Phi_t(12,34,56)\rangle=-\frac{1}{\sqrt{3}} . \tag{A7}$$

Therefore formula (4.21) becomes

$$Z^{BB'}(lS)=-3\sqrt{3}N_m N_t \sum{}''(-)''(-1)^{\tilde{L}}\int [\Phi_t^{BB'}(IlSJ{:}\mathbf{r})]^{\dagger}\tilde{\Phi}_t(l_1 l_2\cdots l_6{:}\mathbf{r})d\Omega , \tag{A8}$$

where $\tilde{\Phi}_t(l_1 l_2 \cdots l_6:\mathbf{r})$ is a function of $\mathbf{r}$ obtained by substituting $\mathbf{r}$ for $\mathbf{r}_i$ in $\Phi_t(l_1 l_2 \cdots l_6)$. Because the 15 terms in (A2) are orthogonal or nearly orthogonal with each other, all values of N_m are equal or nearly equal to $1/\sqrt{15}$. Therefore, in actual calculation, it is convenient to use the quantities

$$D_N = \sqrt{15} N_m \ , \tag{A9}$$

$$\epsilon_D^{BB'}(nlS) = \epsilon^{BB'}(nlS)/D_N \ . \tag{A10}$$

The $\epsilon_D^{BB'}(LlS)s$ for the $1p\frac{1}{2}$-shell dibaryons calculated by formula (A10) are tabulated in Table II together with D_N.

APPENDIX B: TABLE OF COEFFICIENTS $A^{NB}(l_k l_q l_t S_k:lS)$

The coefficients $A^{NB}(l_k l_q l_t S_k:lS)$ in formula (4.30) for major $1p\frac{1}{2}$-shell dibaryons are tabulated in Table III. Note that the calculation of partial decay widths is simplified remarkably by the use of expression (4.30).

APPENDIX C: T MATRIX

In the scattering between particles A and B, we adopt the definition of T matrix as

$$\begin{aligned} T_{fi} &= \delta(E_f - E_i)\langle \mathbf{q}_f \mid V\Omega^+ \mid \mathbf{q}_i \rangle \ , \\ \Omega^+ &= 1 + \frac{1}{E - H + i\epsilon} V \ , \end{aligned} \tag{C1}$$

where V and H represent the interaction between A and B and the total Hamiltonian, respectively, $\mathbf{q}_f$ (E_f) and $\mathbf{q}_i$ (E_i) are the relative momenta (energies) between A and B in final and initial states, respectively. Note that the δ function in (C1) is dropped in conventional definition.

With definition (C1), the S matrix is written as

$$S = 1 - 2\pi i T \ . \tag{C2}$$

From unitarity property $SS^\dagger = 1$, it follows that

$$T - T^\dagger = -2\pi i T T^\dagger \ . \tag{C3}$$

The T matrix $T_{\alpha\beta}(E)$ for exit channel α and entrance channel β with energy $E_i = E$ is obtained from T_{fi} by means of the partial-wave expansion. The result is

$$T_{\alpha\beta}(E) = \frac{1}{(2\pi)^3} \int \delta(E_f - E)\langle \alpha \mid V\Omega^+ \mid \beta \rangle d^3 q_f \ , \tag{C4}$$

where $\langle \alpha \mid V\Omega^+ \mid \beta \rangle$ represents the element for the channel α and β in the partial-wave expansion representation of the matrix element $\langle \mathbf{q}_f \mid V\Omega^+ \mid \mathbf{q}_i \rangle$ using the normalized color-isospin-spin-angular wave functions. The expression (5.11) is obtained by the application of formula (C4) to πd resonating scattering with interaction V_π putting $\mathbf{q}_f = \mathbf{q}$ and $E_f = 2m_N - B + q_0$.

APPENDIX D: ENERGY SHIFT Δ_{TS}

In this appendix we calculate the energy shift Δ_{TS} of a $[(1p\frac{1}{2})(1s\frac{1}{2})]$ diquark with isospin T and spin S assuming that Δ_{TS} is derived from a qq two-body Coulombic interaction H_g, and the residual central qq force H_c (the extra confining potential). Denoting the constituent two quarks by 1 and 2, H_g and H_c can be written as

$$\begin{aligned} H_g &= -\tfrac{2}{3}\alpha_s S_{12} \ , \\ S_{12} &= \frac{1}{r} - \frac{1}{2m^2}\left[\frac{(\mathbf{p}_1\cdot\mathbf{p}_2)}{r} + \frac{\mathbf{r}\cdot(\mathbf{r}\cdot\mathbf{p}_1)\mathbf{p}_2}{r^3}\right] - \frac{8\pi}{3m^2}\delta^3(\mathbf{r})\mathbf{s}_1\cdot\mathbf{s}_2 - \frac{1}{2m^2 r^3}[(\mathbf{r}\times\mathbf{p}_1)\cdot\mathbf{s}_1 - (\mathbf{r}\times\mathbf{p}_2)\cdot\mathbf{s}_2] \\ &\quad - \frac{1}{m^2 r^3}[(\mathbf{r}\times\mathbf{p}_1)\cdot\mathbf{s}_2 - (\mathbf{r}\times\mathbf{p}_2)\cdot\mathbf{s}_1] - \frac{1}{m^3 r^3}\left[\frac{3(\mathbf{s}_1\cdot\mathbf{r})(\mathbf{s}_2\cdot\mathbf{r})}{r^2} - \mathbf{s}_1\cdot\mathbf{s}_2\right] , \end{aligned} \tag{D1}$$

$$H_c = \frac{\gamma m^3 r^2}{4} + C \ , \tag{D2}$$

where $\mathbf{r}$ represents the separation between quarks 1 and 2, α_s is the effective gauge coupling constant, and γ and C are free parameters. The energy shift Δ_{TS} is given by

$$\Delta_{TS} = \langle H_g \rangle + \langle H_c \rangle \ . \tag{D3}$$

By a straightforward calculation, one obtains an expression

$$\Delta_{TS} = -\tfrac{5}{24}\Delta[1 - \bar{\gamma}(-1)^{T+S}][1 + 2(-1)^S] + \bar{C} \ , \tag{D4}$$

$$\Delta = \frac{4}{9}\left[\frac{2}{\pi}\right]^{1/2} \alpha_s \frac{m}{(mR)^3} \ , \tag{D5}$$

where $\bar{\gamma}$ and $\bar{C}$ are the parameters which depend on γ and C.

We present here one interesting modification of expression (D4). Eliminating the tensor force in (D1) and taking

$$\gamma = \frac{\Delta}{m}\left[\frac{15}{2(mR)^2} - 1\right] \tag{D6}$$

with an appropriate value for C, one obtains

$$\Delta_{TS} = -\frac{\Delta}{4}[1 - (-1)^T][1 + (-1)^S] \ . \tag{D7}$$

For $R_\pi = m^{-1}$ and $\Delta = 60$ MeV, the value of α_s and γ becomes

$$\alpha_s = 0.564 \quad \text{and} \quad \gamma = 1.3 \ . \tag{D8}$$

Since the qq confining potential for $\omega = m$ is given by $\frac{1}{4} m^3 r^2$, the extra confining potential is nearly equal to the original one. This result may be reasonable because, from the analysis of P-wave excited baryons, it can be inferred that a strong extra confining potential exists in the $n=1$ excited diquarks. In fact, if one tries to reproduce the large empirical angular frequency $\omega = 520$ MeV for P-wave baryons by including extra confining potential (D2), one obtains $\gamma = 2.0$.

---

[1]We denote the dibaryon candidate by $B_I^2(M)J^P$ where M, I, J, and P represent the dibaryon mass in GeV, isospin, spin and parity, respectively.

[2]See, for example, A. Yokosawa, Phys. Rep. **64**, 47 (1980); A. Švarc, in *Particles and Nuclei,* proceedings of the Tenth International Conference, Heidelberg, 1984, edited by B. Povh and G. zu Palitz (North-Holland, Amsterdam, 1985) [Nucl. Phys. **A434**, 329c (1985)]; M. P. Locher, M. E. Sainio, and A. Švarc, SIN Report No. PR-85-12, 1985 (unpublished).

[3]A. Yokosawa, in *Proceedings of Sixth International Symposium on Polarization Phenomena in Nuclear Physics, Osaka, 1985,* edited by M. Kondo *et al.* [J. Phys. Soc. Jpn. Suppl. **55**, 251 (1986)].

[4]R. R. Silber and W. M. Kloet, Nucl. Phys. **A338**, 3 (1980); W. M. Kloet and R. R. Silber, *ibid.* **A364**, 346 (1981).

[5]T. Ueda, Phys. Lett. **114B**, 281 (1982); **141B**, 157 (1984); J. Phys. Soc. Jpn. Suppl. **55**, 846 (1986).

[6]P. J. G. Mulders, A. T. M. Aerts, and J. J. de Swart, Phys. Rev. Lett. **40**, 1543 (1978); A. T. M. Aerts *et al.*, Phys. Rev. D **17**, 260 (1978); P. J. G. Mulders *et al.*, *ibid.* **D21**, 2653 (1980).

[7]M. Imachi *et al.*, Prog. Theor. Phys. **55**, 551 (1976); **57**, 517 (1977).

[8]S. Ishida and M. Oda, Prog. Theor. Phys. **60**, 828 (1978); **61**, 1401 (1979).

[9]G. F. Chew and C. Rosenzweig, Phys. Rep. **41**, 263 (1978).

[10]H. Nakamura, K. Arita, and K. Mori, Lett. Nuovo Cimento **21**, 337 (1978); N. Konno, *ibid.* **31**, 401 (1981).

[11]N. Konno and H. Nakamura, Lett. Nuovo Cimento **34**, 313 (1982); N. Konno, Ph.D. thesis Aoyama Gakuin University, 1983; N. Konno, H. Nakamura, and H. Noya, J. Phys. Soc. Jpn. Suppl. **55**, 844 (1986).

[12]I. P. Auer *et al.*, Phys. Rev. Lett. **41**, 354 (1978).

[13]N. Hoshizaki, Prog. Theor. Phys. **60**, 1796 (1978); **61**, 129 (1979).

[14]N. Hoshizaki, new phase shift cited in Ref. 3, p. 258, Fig. 9.

[15]N. Hidaka *et al.*, Phys. Lett. **70B**, 479 (1977).

[16]J. Bolger *et al.*, Phys. Rev. Lett. **46**, 167 (1981); **48**, 1667 (1982).

[17]G. R. Smith *et al.*, Phys. Rev. D **29**, 2206 (1984).

[18]E. Ungricht *et al.*, Phys. Rev. Lett. **52**, 333 (1984).

[19]Y. M. Shin *et al.*, Phys. Rev. Lett. **55**, 2672 (1985).

[20]J. Ulbricht *et al.*, Phys. Rev. Lett. **48**, 311 (1982); W. Grüebler *et al.*, *ibid.* **49**, 444 (1982); V. König *et al.*, J. Phys. G **9**, L121 (1983).

[21]M. Merdzen *et al.*, J. Phys. Soc. Jpn. Suppl. **55**, 842 (1986).

[22]I. P. Auer *et al.*, Phys. Rev. Lett. **46**, 1177 (1981).

[23]K. Hashimoto, Y. Higuchi, and N. Hoshizaki, Prog. Theor. Phys. **64**, 1678 (1980); K. Hashimoto and N. Hoshizaki, *ibid.* **64**, 1693 (1980).

[24]B. Tatischeff *et al.*, Phys. Rev. Lett. **52**, 2022 (1984).

[25]T. Siemiarczuk, J. Stepaniak, and P. Zieliński, Phys. Lett. **128B**, 367 (1983).

[26]J. S. Chalmers *et al.*, J. Phys. Soc. Jpn. Suppl. **55**, 910 (1986).

[27]D. B. Lichtenberg *et al.*, Phys. Rev. D **18**, 256 (1978).

[28]A. De Rújula, H. Georgi, and S. L. Glashow, Phys. Rev. D **12**, 1147 (1975).

[29]K. Hirata *et al.*, Phys. Rev. D **18**, 834 (1978).

[30]N. Isgur and G. Karl, Phys. Rev. D **18**, 4187 (1978); **19**, 2653 (1979).

[31]NN spin-triplet $J = L =$ odd state.

[32]I. P. Auer *et al.*, Phys. Rev. Lett. **48**, 1150 (1980).

[33]T. Kamae *et al.*, Phys. Rev. Lett. **38**, 468 (1977).

[34]A. Ui and K. Saito, Prog. Theor. Phys. **69**, 1467 (1983).

[35]A. Chodos and C. B. Thorn, Phys. Rev. D **12**, 2733 (1975).

[36]G. E. Brown and M. Rho, Phys. Lett. **82B**, 177 (1979); **84B**, 383 (1979); V. Vento *et al.*, Nucl. Phys. **A345**, 413 (1980); G. E. Brown, M. Rho, and V. Vento, Phys. Lett. **97B**, 423 (1980); V. Vento, M. Rho, and G. E. Brown, *ibid.* **103B**, 285 (1981); V. Vento, *ibid.* **107B**, 5 (1981); F. Myhrer, G. E. Brown, and Z. Xu, Nucl. Phys. **A362**, 317 (1981); I. Hulthage, F. Myhrer, and Z. Xu, *ibid.* **A364**, 322 (1981).

[37]I. Inoue and T. Maskawa, Prog. Theor. Phys. **54**, 1833 (1975); A. W. Thomas, S. Théberge, and G. A. Miller, Phys. Rev. D **22**, 2838 (1980); **24**, 216 (1981); C. DeTar, *ibid.* **24**, 752 (1981); **24**, 762 (1981).

[38]K. Kubodera and M. P. Locher, Phys. Lett. **87B**, 169 (1979); K. Kubodera *et al.*, J. Phys. G **6**, 171 (1980).

[39]W. P. Madigam *et al.*, Phys. Rev. D **31**, 966 (1985).

[40]N. Hoshizaki, in *Proceedings of the II Meeting on Exotic Resonances, Hiroshima, 1980,* edited by I. Endo and *et al.* (Hiroshima University Report No. HUPD-8010), pp 1—19.